



# Coupled Van der Pol oscillators

Giulio Ghirardo

Downing College

1st year report for the Degree of Doctor of Philosophy



# Contents

<b>1</b>	<b>Single Van Der Pol Oscillator</b>	<b>5</b>
1.1	Standard form . . . . .	6
1.2	Method of averaging . . . . .	8
1.3	Tuning of the VdP to experiments . . . . .	11
1.4	Single forced VDP . . . . .	13
1.4.1	Harmonic forcing . . . . .	13
1.4.1.1	Analytical entrainment criterion . . . . .	13
1.4.1.2	Simulation results . . . . .	16
1.4.2	Random forcing . . . . .	26
<b>2</b>	<b>Coupled Van der Pol oscillators</b>	<b>29</b>
2.1	The model . . . . .	29
2.2	Linear analysis . . . . .	31
2.2.1	Effect of the coupling on the stability . . . . .	33
2.3	Introductory simulation results . . . . .	36
2.4	Method of averaging . . . . .	42
2.4.1	Entrained Solution . . . . .	43
2.4.1.1	General solution . . . . .	46
2.4.1.2	Study of regularity of the perturbation problem . . . . .	47
2.4.2	Distinct oscillators . . . . .	48
2.5	Discussion of the solution . . . . .	50
2.5.1	Dependence on the distance from the origin . . . . .	50
2.5.2	The case of velocity coupling . . . . .	54
2.5.3	Limit-cycle amplitudes for the velocity coupling case . . . . .	57
	<b>Bibliography</b>	<b>63</b>



# Chapter 1

## Single Van Der Pol Oscillator

This chapter investigates the Van der Pol oscillator (VDP) as a simple prototype of global modes in physics, with a focus in fluid mechanics. The VDP is the simplest nonlinear oscillator, discovered by Van Der Pol [7] in electric circuits. The VDP model is a second order differential equation,

$$\ddot{x} + \omega\varepsilon(x^2 - 1)\dot{x} + \omega^2x = 0, \quad (1.1)$$

where  $\omega$  is the natural<sup>1</sup> frequency of the system,  $\varepsilon > 0$  the coefficient regulating the nonlinearity, and the dot indicating the derivative with respect to a time variable  $t$ . Operating a change of variable  $\tau = \omega t$ ,

$$\ddot{x} + \varepsilon(x^2 - 1)\dot{x} + x = 0, \quad (1.2)$$

we obtain the standard form of the VDP, a one-parameter nonlinear differential equation of the second order. In all the following treatise we study VDPs and systems of VDPs with the nonlinear parameter  $\varepsilon$  smaller than 0.1. This has an empirical but solid motivation, regarding the time series of the phenomena we want to model. All the signals investigated so far, and their derivatives, show harmonic behavior, without abrupt discontinuities. In the same way, the VDP presents abrupt discontinuities for relatively high values of  $\varepsilon$ , while its solutions become smoother for smaller values of  $\varepsilon$ .

---

<sup>1</sup>the frequency of the system for  $\varepsilon = 0$

The second order equation (1.2) can be rewritten as a first order system:

$$\begin{cases} \dot{x} = y \\ \dot{y} = -\varepsilon(x^2 - 1)y - x \end{cases}, \quad \begin{cases} x(0) = x_0 \\ y(0) = y_0 \end{cases}. \quad (1.3)$$

The system presents a single fixed point,  $(x, y) = (0, 0)$ . A linear analysis of the fixed point leads to the two following eigenvalues,

$$\lambda_{1,2} = \frac{\varepsilon}{2} \pm i\sqrt{1 - \frac{\varepsilon^2}{4}}, \quad (1.4)$$

indicating the fixed point is an unstable focus for  $\varepsilon < 2$ , that is our case.

## 1.1 Standard form

A closer look at the system (1.3) reveals that it is a perturbation problem in  $\varepsilon$ , and that it is quasilinear, since it can be rewritten in the form

$$\begin{cases} \dot{\mathbf{x}} = \mathbf{A}\mathbf{x} + \varepsilon\mathbf{f}^1(\mathbf{x}, t) \\ \mathbf{x}(0) = \mathbf{x}_0 \end{cases}, \quad (1.5)$$

with

$$\mathbf{x} = \begin{bmatrix} x \\ y \end{bmatrix} \quad \mathbf{A} = \begin{bmatrix} 0 & 1 \\ -1 & 0 \end{bmatrix} \quad \mathbf{f}^1 = \begin{bmatrix} 0 \\ -(x^2 - 1)y \end{bmatrix} \quad (1.6)$$

The unperturbed problem is obtained setting  $\varepsilon = 0$ ,

$$\begin{cases} \dot{\mathbf{y}} = \mathbf{A}\mathbf{y} \\ \mathbf{y}(0) = \mathbf{x}_0 \end{cases} \quad (1.7)$$

leading to the solution

$$\begin{cases} \mathbf{y}(t) = e^{\mathbf{A}t}\mathbf{x}_0 = \mathbf{\Phi}(t)\mathbf{x}_0 \\ \mathbf{\Phi}(t) = [\mathbf{y}_1^T(t), \mathbf{y}_2^T(t)] \end{cases}, \quad (1.8)$$

where  $\mathbf{y}_1, \mathbf{y}_2$  are the two linearly independent solutions

$$\begin{cases} \mathbf{y}_1(t) = (\cos t, \sin t) \\ \mathbf{y}_2(t) = (-\sin t, \cos t) \end{cases}. \quad (1.9)$$

We observe that  $\Phi(0) = \mathbf{I}_{2 \times 2}$  and that equation (1.8.a) can be rewritten with a direct dependence on the original condition, as

$$\begin{cases} \mathbf{y}(\mathbf{x}_0, t) = \Phi(t)\mathbf{x}_0 \\ \mathbf{y}(\mathbf{x}_0, 0) = \mathbf{x}_0 \end{cases}. \quad (1.10)$$

We now look for a solution of the original perturbed problem (1.5) with a similar structure to (1.10):

$$\begin{cases} \mathbf{x}(\zeta(t), t) = \Phi(t)\zeta(t) \\ \zeta(0) = \zeta_0 = \mathbf{x}_0 \end{cases} \quad (1.11)$$

Substituting (1.11.a) in (1.5), we obtain

$$\dot{\Phi}\zeta + \Phi\dot{\zeta} = A\Phi\zeta + \varepsilon f^1(\Phi\zeta, t) \quad (1.12)$$

$$(\dot{\Phi} - A\Phi)\zeta + \Phi\dot{\zeta} = \varepsilon f^1(\Phi\zeta, t) \quad (1.13)$$

Now the first term disappears because of how  $\Phi$  is defined in (1.8). Since  $\Phi$  is invertible, we then obtain:

$$\begin{cases} \dot{\zeta} = \varepsilon \Phi(t)^{-1} \mathbf{f}^1(\Phi(t)\zeta(t), t) \\ \zeta(0) = \zeta_0 \end{cases}. \quad (1.14)$$

This is now a regular perturbation problem in the variable  $\zeta$ , known as the standard form of the original quasilinear problem (1.5). From equation (1.11.a), we observe that  $\zeta$  modulates the solutions of the unperturbed linear problem that appear in the matrix  $\Phi$ . Working out equation (1.14.a), we obtain

$$\frac{\dot{\zeta}}{\varepsilon} = \begin{bmatrix} -c^2 s^2 \zeta_1^3 - c^3 s \zeta_1^2 \zeta_2 - s^4 \zeta_1 \zeta_2^2 - s^3 c \zeta_2^3 - 2cs^3 \zeta_1^2 \zeta_2 - 2c^2 s^2 \zeta_1 \zeta_2^2 + s^2 \zeta_1 + cs \zeta_2 \\ -c^3 s \zeta_1^3 - c^4 \zeta_1^2 \zeta_2 - cs^3 \zeta_1 \zeta_2^2 - s^2 c^2 \zeta_2^3 - 2c^2 s^2 \zeta_1^2 \zeta_2 - 2c^3 s \zeta_1 \zeta_2^2 + cs \zeta_1 + c^2 \zeta_2 \end{bmatrix} \quad (1.15)$$

where  $c = \cos t$  and  $s = \sin t$ .

It is possible to choose an alternative structure for the solution of the linear problem (1.7). Instead of equations (1.8,1.9,1.11), we study the linear solution in terms of a phase  $\varphi$  and amplitude  $r$ . The equation corresponding to (1.11) is

$$\mathbf{x}(\zeta(t), t) = \begin{bmatrix} r(t) \sin(t - \varphi(t)) \\ r(t) \cos(t - \varphi(t)) \end{bmatrix} \quad \zeta = \begin{bmatrix} r \\ \varphi \end{bmatrix} \quad (1.16)$$

$$\zeta(0) = \begin{bmatrix} \sqrt{x_0^2 + y_0^2} \\ \tan^{-1}(-y_0/x_0) \end{bmatrix} \equiv \zeta_0 \quad (1.17)$$

As done before, substituting (1.16) in (1.3), we obtain:

$$\begin{cases} \dot{r}s - rc\dot{\varphi} = \varepsilon f_1^1 \equiv 0 \\ \dot{r}c + rs\dot{\varphi} = \varepsilon f_2^1 \equiv -\varepsilon(r^2s^2 - 1)rc \end{cases}, \quad (1.18)$$

where  $s = \sin(t - \varphi)$  and  $c = \cos(t - \varphi)$ . Elaborating further from (1.18), we obtain

$$\begin{bmatrix} \dot{r} \\ \dot{\varphi} \end{bmatrix} = \varepsilon \begin{bmatrix} -rc^2(r^2s^2 - 1) \\ -cs(r^2s^2 - 1) \end{bmatrix} = \varepsilon \mathbf{g}(\zeta, t) \quad (1.19)$$

Equations (1.15) and (1.19), with the respective initial conditions (1.11.b) and (1.17), are two equivalent formulations of the standard form of the VdP. If  $\zeta(t)$  is known, the exact solution  $\mathbf{x}(t)$  can be derived with (1.11) or (1.16), depending on the formulation.

## 1.2 Method of averaging

Both equations (1.15) and (1.19) are now in standard form, i.e.

$$\dot{\zeta} = \varepsilon \mathbf{g}(\zeta, t), \quad (1.20)$$

where the dependence on  $t$  of  $g$  is due to  $\Phi(t)$ . We now observe that  $\mathbf{f}^1$  is periodic in  $t$  with period  $T = 2\pi$ , and we can proceed applying the method of averaging

on this system. We introduce the averaging operator,

$$\bar{\zeta}(t) = \frac{1}{2\pi} \int_{t-\pi}^{t+\pi} \zeta(u) du, \quad (1.21)$$

$$\bar{\mathbf{g}}(\zeta(t), t) = \frac{1}{2\pi} \int_{t-\pi}^{t+\pi} \mathbf{g}(\zeta(u), u) du \quad (1.22)$$

and clearly it follows<sup>2</sup> that

$$\dot{\bar{\zeta}} = \varepsilon \bar{\mathbf{g}}(\zeta, t). \quad (1.23)$$

Moreover, we observe that

$$\bar{\zeta}(t) = \frac{1}{2\pi} \int_{t-\pi}^{t+\pi} \zeta(t) - [\zeta(t) - \zeta(s)] ds \quad (1.24)$$

We apply now a Taylor series on  $\zeta(s)$  around  $s = t$ ,

$$\zeta(s) = \zeta(t) + \sum_{j=1}^{\infty} \frac{\zeta^{(j)}(t)}{j!} (s-t)^j \quad (1.25)$$

and, employing (1.20) on the derivatives of  $\zeta$ , we obtain

$$\zeta(s) = \zeta(t) + \varepsilon \sum_{j=1}^{\infty} \frac{\mathbf{g}^{(j-1)}(t)}{j!} (s-t)^j = \zeta(t) + O(\varepsilon). \quad (1.26)$$

Substituting this Taylor expansion in (1.24),

$$\bar{\zeta}(t) = \zeta(t) - \varepsilon \frac{1}{2\pi} \int_{t-\pi}^{t+\pi} \sum_{j=1}^{\infty} \zeta^{(j)}(t) \frac{(s-t)^j}{j!} ds, \quad (1.27)$$

or in other words

$$\zeta(t) = \bar{\zeta}(t) + O(\varepsilon) \quad (1.28)$$

---

<sup>2</sup>it is simple to prove that the average operator and the time-derivative commute

Applying now a Taylor expansion on  $\mathbf{g}$  with respect to  $\boldsymbol{\zeta}$ , and taking into account (1.28), it can be proved that

$$\bar{\mathbf{g}}(\boldsymbol{\zeta}(t), t) = \bar{\mathbf{g}}(\bar{\boldsymbol{\zeta}}, t) + O(\varepsilon). \quad (1.29)$$

We now emphasise that

$$\bar{\mathbf{g}}(\bar{\boldsymbol{\zeta}}, t) = \frac{1}{2\pi} \int_{t-\pi}^{t+\pi} \mathbf{g}(\bar{\boldsymbol{\zeta}}(t), u) du, \quad (1.30)$$

and that in this expression the quantity  $\bar{\boldsymbol{\zeta}}$  is a constant in the integral. Substituting finally this equation in (1.23), we have

$$\dot{\bar{\boldsymbol{\zeta}}} = \varepsilon \bar{\mathbf{g}}(\bar{\boldsymbol{\zeta}}, t) + O(\varepsilon^2) \quad (1.31)$$

Usually we refer to the averaged variables  $\boldsymbol{\zeta} = (\bar{r}, \bar{\phi})$  as slow variables, and the flow specified by (1.31) dropping the higher terms in  $\varepsilon$  as the slow flow. Moreover, since there is no simple way to calculate  $(r, \phi)$ , it is common practice to indicate the averaged quantities without overlining them.

Dropping the bars, the equation (1.31) for the single VdP, substituting from (1.19) the expression for  $\mathbf{g}$ , becomes

$$\begin{bmatrix} \dot{r}(t) \\ \dot{\varphi}(t) \end{bmatrix} = \frac{\varepsilon}{2\pi} \int_{t-\pi}^{t+\pi} \begin{bmatrix} -r(t) \cos(u - \varphi(t))^2 [r(t)^2 \sin(u - \varphi(t))^2 - 1] \\ \cos(u - \varphi(t)) \sin(u - \phi(t)) [r(t)^2 \sin(u - \varphi(t))^2 - 1] \end{bmatrix} du$$

In the expression, we have preferred to explicitly indicate the dependence on  $t$  and on  $u$  of the variables. We also note that the period of averaging may be in general different from  $T = 2\pi$ . Changing variable in the integral choosing  $v = u - \varphi(t)$ , we have  $dv = du$ . Being the integrand periodic in  $u$  and then in  $v$ , we also change the extremes of integration from  $[t - \varphi(t) - \pi, t - \varphi(t) + \pi]$  to  $[0, \pi]$ . We obtain

$$\begin{bmatrix} \dot{r}(t) \\ \dot{\varphi}(t) \end{bmatrix} = \frac{\varepsilon}{2\pi} \int_0^{2\pi} \begin{bmatrix} -r(t) \cos^2 v (r(t)^2 \sin^2 v - 1) \\ \cos v \sin v (r(t)^2 \sin^2 v - 1) \end{bmatrix} dv \quad (1.32)$$

The final result is

$$\begin{cases} \dot{r} = \varepsilon \frac{r}{2} \left[ 1 - \left( \frac{r}{2} \right)^2 \right] \\ \dot{\varphi} = 0 \end{cases} \quad (1.33)$$

From (1.33), it is apparent that the phase is constant, and

- For  $\varepsilon > 0$ , we have a stable solution, with limit cycle amplitude  $A \equiv \bar{r} = 2$
- For  $\varepsilon < 0$ , the only stable point is  $r = 0$ , and the solution may diverge to infinity for large enough initial conditions. We will discuss this undesired behavior of the VdP in section 1.3.

Sometimes we deal with the more general equation

$$\ddot{x} + \varepsilon(\alpha x^2 - \beta)\dot{x} + x = 0 \quad (1.34)$$

In this case, the slow flow is

$$\begin{cases} \dot{r} = \varepsilon \frac{r}{2} \left[ \beta - \alpha \left( \frac{r}{2} \right)^2 \right] \\ \dot{\varphi} = 0 \end{cases} \quad (1.35)$$

The limit-cycle amplitude is in that case

$$A = 2\sqrt{\beta/\alpha} \quad (1.36)$$

### 1.3 Tuning of the VdP to experiments

We are interested in tuning the VdP model to linear modes of oscillation. Two important results of stability analyses are the linear growth-rate  $\sigma$  and the linear natural frequency  $\omega_L$  of the linear mode. A linear stability analysis of system (1.1) leads to the nondimensionalised version of equation (1.4),

$$\lambda_{1,2} = \frac{\varepsilon\omega}{2} \pm i\sqrt{1 - \frac{\varepsilon^2}{4}}\omega = \sigma + i\omega_L. \quad (1.37)$$

Inverting this relation, we can work out

$$\begin{cases} \omega = \sqrt{\omega_L^2 + \sigma^2} \\ \varepsilon = \frac{2\sigma}{\sqrt{\omega_L^2 + \sigma^2}} \end{cases} . \quad (1.38)$$

Observe that for a stable mode we have  $\sigma < 0$ , and consistently from equation (1.37) the origin is an attractor. Still, for large initial conditions on  $(x, \dot{x})$  the solution diverges to infinity due to the quadratic term. This behavior of the VdP is not consistent with the behavior of stable global modes, that decay to zero for any perturbation. To settle this problem, we modify the VdP model as

$$\ddot{x} + \varepsilon(\text{sgn}(\varepsilon)x^2 - 1)\dot{x} + x = 0. \quad (1.39)$$

Observe that since the adjustment is on the nonlinear term, the linear analysis remains unchanged. We will keep this change to the model through all the dissertation. This modified model is equivalent to a less popular version of the VdP oscillator, presented in the form:

$$\ddot{y} + (y^2 - \lambda)\dot{y} + y = 0. \quad (1.40)$$

Substituting  $x = \sqrt{|\lambda|}y$  in (1.40), we obtain equation (1.39) with  $\varepsilon = \lambda$ . We opt for the model described by equation (1.39) because in that model the final amplitude of oscillation doesn't depend on  $\lambda$ . In the following, with a small abuse of nomenclature, we will refer to (1.39) with negative  $\varepsilon$  as a stable VdP, referring to the case of positive  $\varepsilon$  as self-excited VdP. There is clearly a parallel with stable and unstable linear modes respectively.

At a first glance, there seems to be little to investigate for negative  $\varepsilon$ , since the solution decays to zero. Nonetheless, we will show that two stable VdPs can become unstable if coupled. This is promising, and consistent with [6].

**The impossibility of tuning the nonlinear term separately.** Equation (1.38) shows how, for very unstable modes with large  $\sigma$ , a large value of the nonlinear coefficient  $\varepsilon$  is predicted, and then a strong nonlinear behavior is expected, as discussed in section 1. We may be tempted to consider a second modified version of the VdP, such that the nonlinear coefficient may be chosen independently

from the expression (1.38):

$$\ddot{x} + \varepsilon_{nl}x^2\dot{x} - \varepsilon\dot{x} + x = 0. \quad (1.41)$$

As a consequence, for the case of positive  $\varepsilon$ , the limit-cycle amplitude from equation (1.36) becomes  $A = 2\sqrt{\varepsilon/\varepsilon_{nl}}$ . But operating the change of variable  $y = \sqrt{|\varepsilon|/\varepsilon_{nl}}x$ , we obtain again the system (1.39), with a large nonlinear term  $\varepsilon_{nl} = |\varepsilon|$ .

This has strong implications on the validity of our model. We know that the VdP presents smooth solutions for small values of  $\varepsilon$ , and we have then restricted  $\varepsilon$  in the range  $0 < \varepsilon \ll 1$ . Conversely, from equation (1.38) we must restrict the validity of our model to the study of modes lightly stable or unstable, with  $|\sigma|$  close to zero.

## 1.4 Single forced VdP

In this section we investigate the behavior of a single VdP subject to external forcing, specifically harmonic and random forcing. In the first scenario, we will discuss frequency entrainment, i.e. when the oscillator pulsates at the same frequency of the forcing, and quasi-periodicity of the solution, i.e. when we assist to a slow scale variation of the orbit of the limit-cycle. We won't cover chaotic behavior of the VdP, since it manifests itself for higher values of the nonlinear parameter  $\varepsilon$ .

In the second scenario, we will show how a stable VdP fed by random noise tends to oscillate at its natural frequency.

### 1.4.1 Harmonic forcing

#### 1.4.1.1 Analytical entrainment criterion

We consider a self-excited VdP subject to harmonic forcing,

$$\ddot{x} + \varepsilon(x^2 - 1)\dot{x} + x = \Gamma \cos \omega t. \quad (1.42)$$

We are expecting that for  $\omega$  close enough to 1, and for large enough  $\Gamma$ , the oscillator will start oscillating at the angular frequency  $\omega$ . We call this phenomena

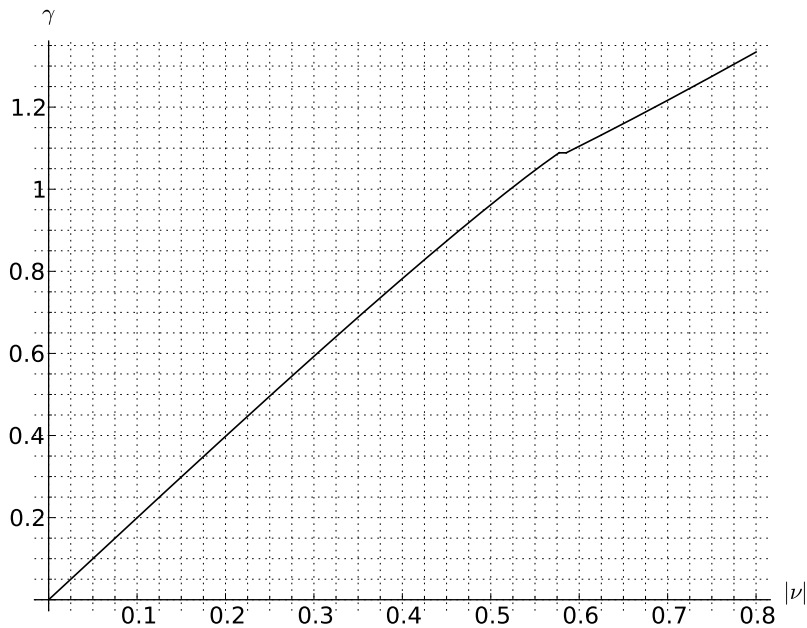


Figure 1.1: Frequency entrainment nondimensionalised criterion, independent of  $\varepsilon$ . Above the curve, the oscillator manifests entrainment.

frequency entrainment, or lock-in. To determine this critical, possible value of  $\Gamma(\omega)$ , we look for an entrained solution

$$x(t) = a(t) \cos \omega t + b(t) \sin \omega t. \quad (1.43)$$

Substituting this trial solution in (1.42), we can investigate a differential system in the new variables  $a$  and  $b$ . If there are any stable solutions for  $a$  and  $b$ , then from equation (1.43) the VdP is entrained. If not, the system is not entrained. We won't report the lengthy analysis, refer to [3] for a good treatise. It is convenient to introduce the nondimensionalised forcing and frequency as

$$\begin{cases} \gamma = \Gamma/\varepsilon\omega \\ \nu = \frac{\omega^2-1}{\varepsilon\omega} \end{cases} \quad (1.44)$$

In figure 1.1 we report the critical value of  $\gamma$  above which we have entrainment, as a function of  $|\nu|$ . To investigate if the nondimensionalisation (1.44) hides any peculiarity, we show the entrainment criterion in the variables  $(\Gamma, \omega)$ , for different values of  $\varepsilon$ . It is clear in figure 1.2 that for the range of the nonlinear

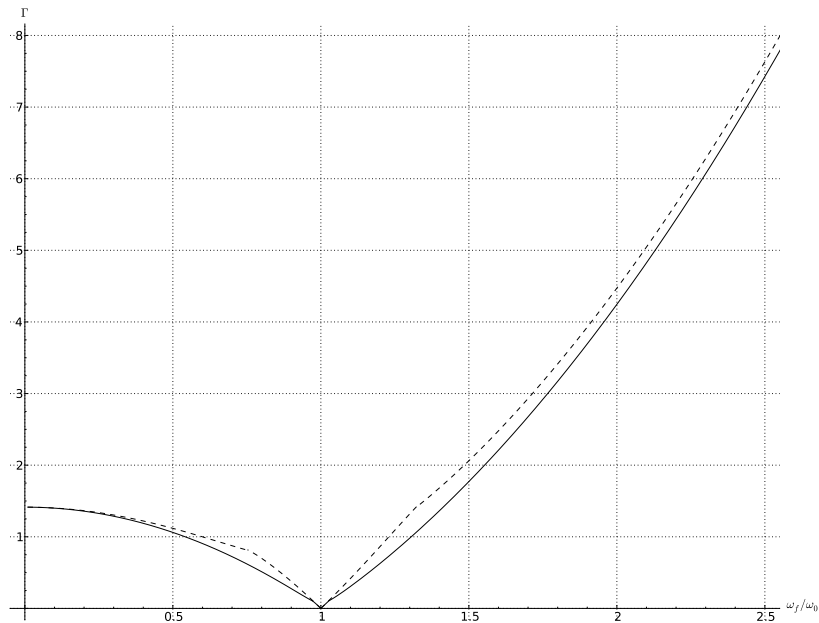


Figure 1.2: Frequency entrainment nondimensionalised criterion. Above the curve, the oscillator manifests entrainment. The dashed curve is for  $\varepsilon = 0.1$ , and the continuous line for  $\varepsilon = 1$ . For values of  $\varepsilon$  smaller than 0.1 there is no apparent change.

parameter investigated,  $\varepsilon$  only slightly affects the behaviour of the VdP subject to forcing. The entrainment curve is a characteristic V-shaped curve, found in many experiments, like [4]. This analytical criterion is valid for  $\omega$  close to 1, and for relatively small values of  $\Gamma$ . In the next section we will discuss how it compares with the simulations. Another aspect we have investigated is the asymmetry of the entrainment V-curve. In figure 1.3 we have reflected the part of the plot on the left of  $\omega = 1$  to the right. The asymmetry of the V is apparent. Some time was spent in trying modified version of the VdP leading to different inclination of the two branches of the V around the point  $(1, 0)$ , with no success. The approach was to change the nonlinear term in equation (1.42),  $n(x) = (x^2 - 1)$ , to something different. The following choices didn't lead to any success:

$$n(x) = |x - 1|; \quad n(x) = |x|^3 - 1; \quad n(x) = x^{2\alpha} - 1. \quad (1.45)$$

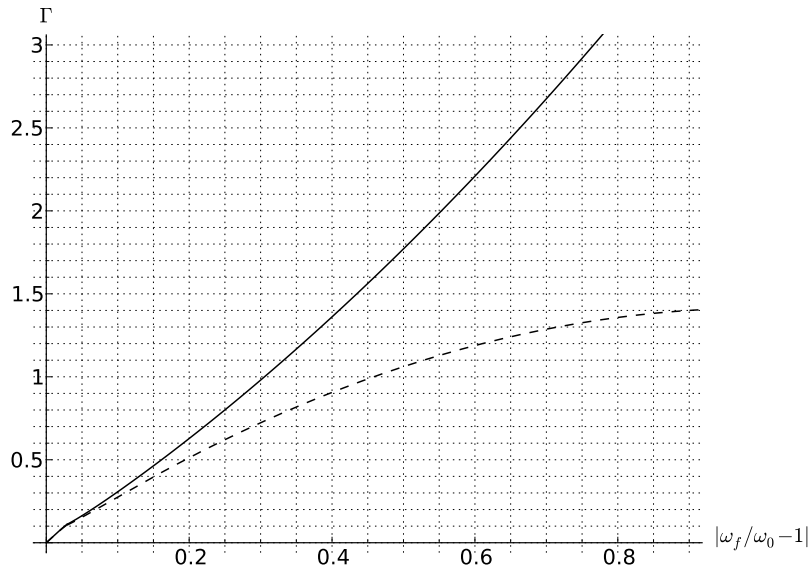


Figure 1.3: Frequency entrainment curve asymmetry. The dashed curve refers to values of  $\omega$  smaller than one, while the continuous line shows the curve for  $\omega$  larger than one. There is a substantial asymmetry.

#### 1.4.1.2 Simulation results

All the simulations were carried on employing a Runge-Kutta fourth-order scheme, with an integration timestep  $\Delta t = 0.05$ . This choice is valid as long as small values of the initial conditions are considered, of the order  $O(10)$ . In figure 1.4 and 1.5 we present the time series and spectra of a VdP for increasing values of the forcing amplitude  $\Gamma_f$ , at a forcing frequency  $\omega_f$  slightly smaller than the natural frequency of the oscillator,  $\omega_f = 0.95$ . For small values of  $\Gamma_f$  the system shows quasi-periodic behavior, with the forcing modulating the amplitude of the limit-cycle of the oscillator in figure 1.4. Above a certain value the VdP is completely entrained with the forcing, with no other peaks appearing in the spectrum in figure 1.5. It is a peculiar characteristic of a VdP oscillator to show smaller peaks on odd harmonics of its natural frequency, i.e. at  $\omega = \{3, 5, 7, \dots\}$ , or at  $\omega = \{3\omega_f, 5\omega_f, 7\omega_f, \dots\}$  in the entrained case.

In figures 1.6 and 1.7 we present the same results for a frequency slightly bigger than 1, setting  $\omega_f = 1.05$ . The results are similar to the previous case.

Consistently with the analytical frequency entrainment criterion previously discussed, for values of  $\omega_f$  further away from 1 the critical value of  $\Gamma_f$  that leads to entrainment grows. This can be observed in figures 1.8,1.9 and 1.10,1.11 for

$\omega_f = 1.3$  and  $\omega_f = 0.7$  respectively.

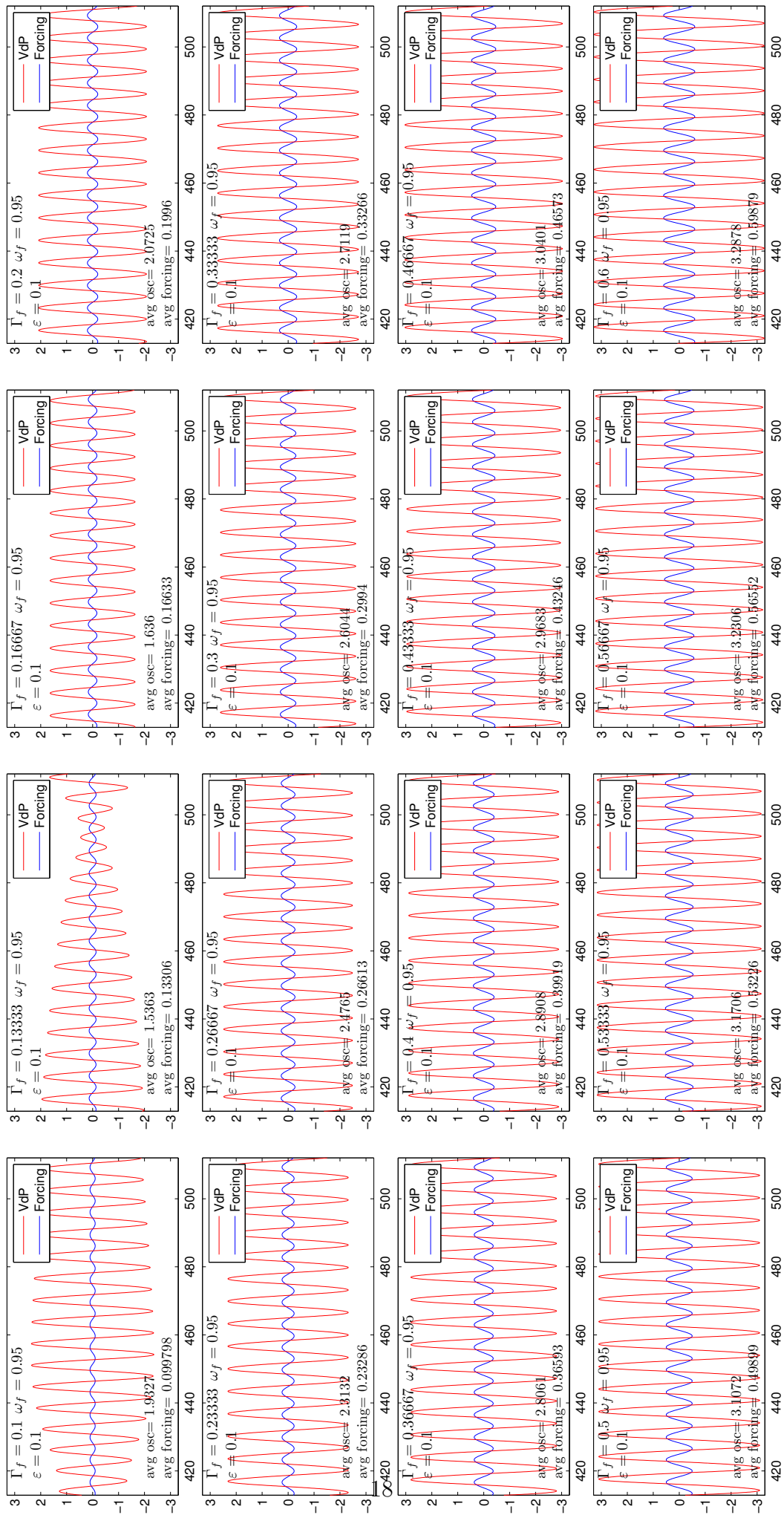


Figure 1.4: Time series of a VdP subject to increasing values of harmonic forcing at frequency  $\omega_f = 0.95$

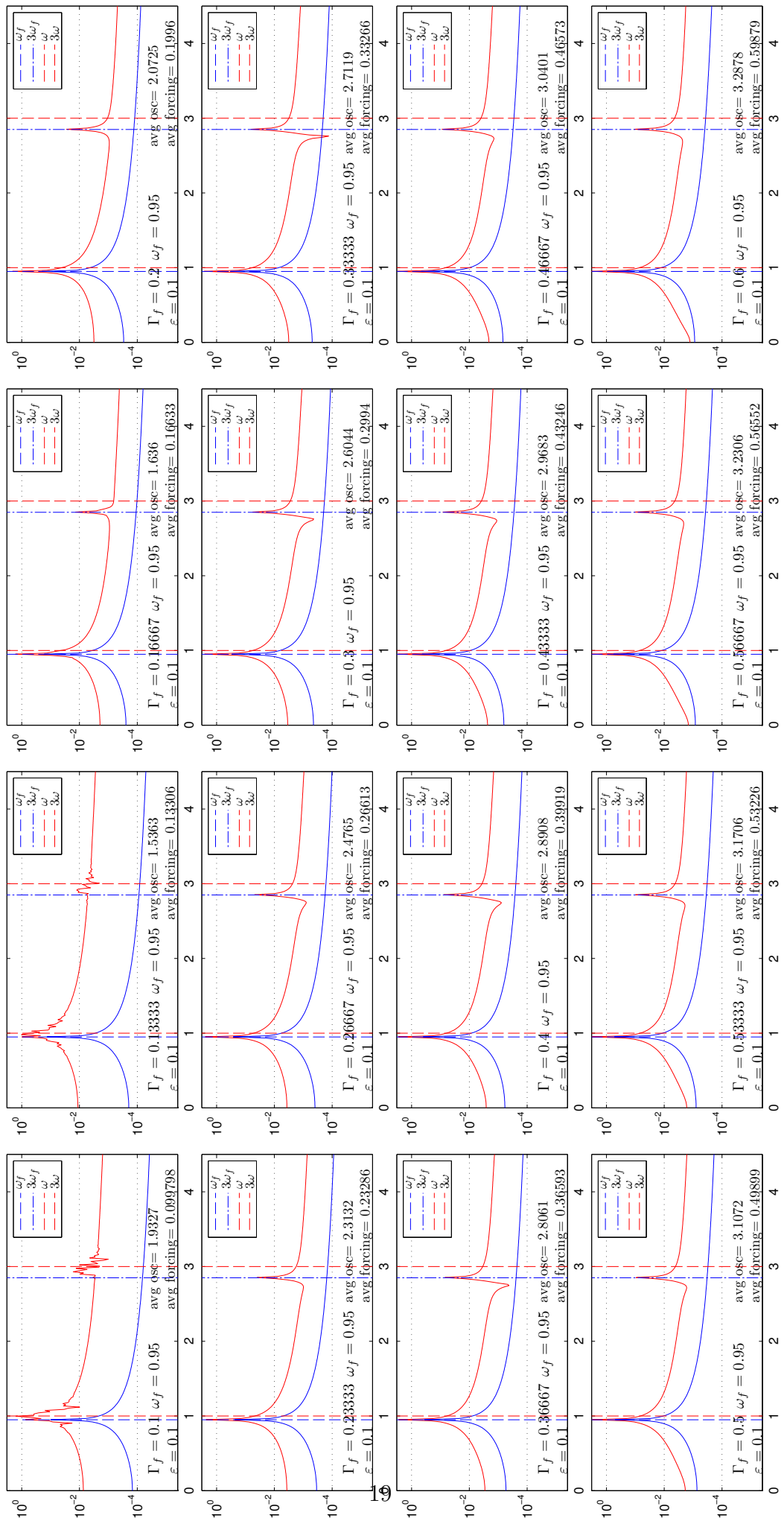


Figure 1.5: Spectrum of a VdP subject to increasing values of harmonic forcing at frequency  $\omega_f = 0.95$

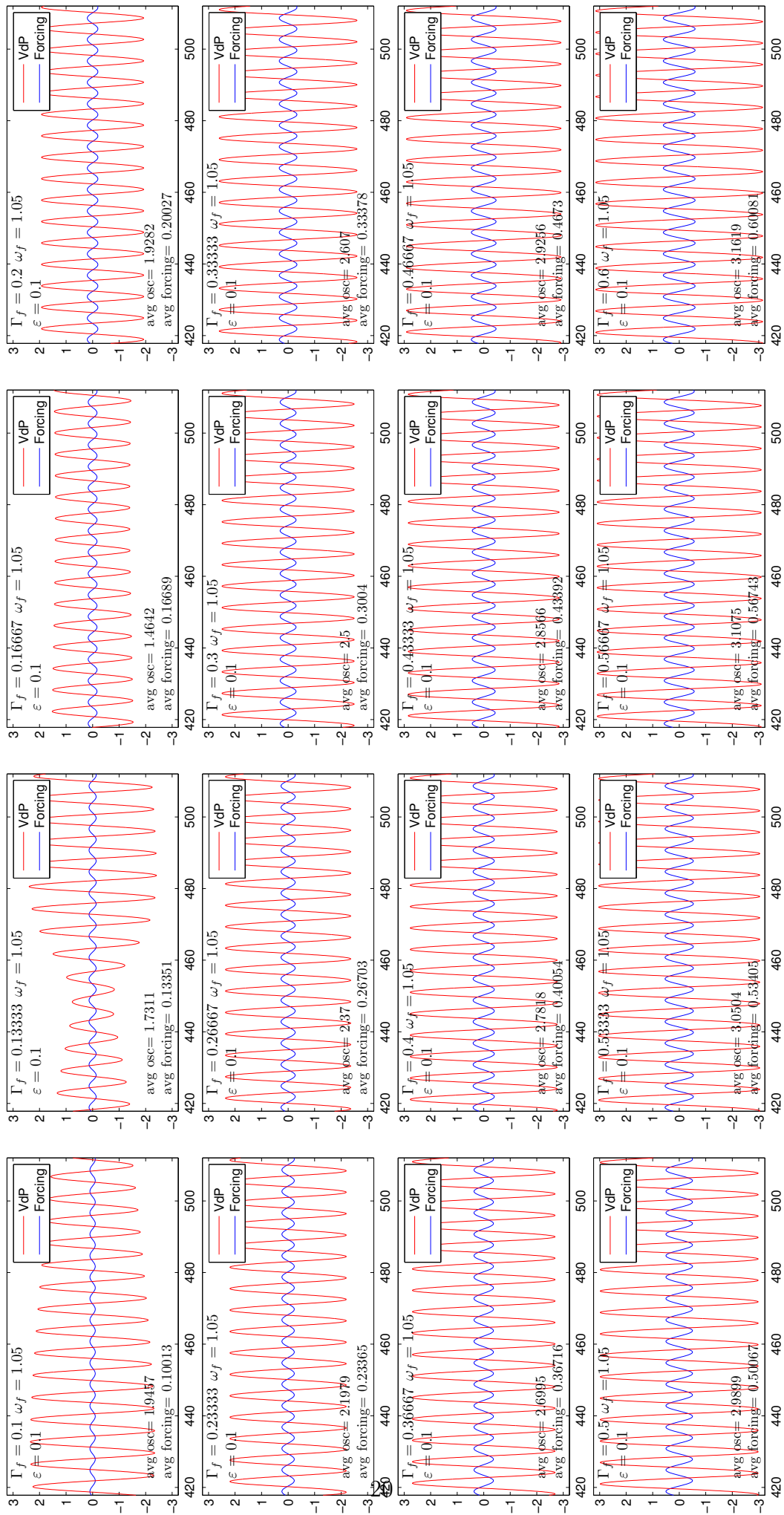


Figure 1.6: Time series of a VdP subject to increasing values of harmonic forcing at frequency  $\omega_f = 1.05$

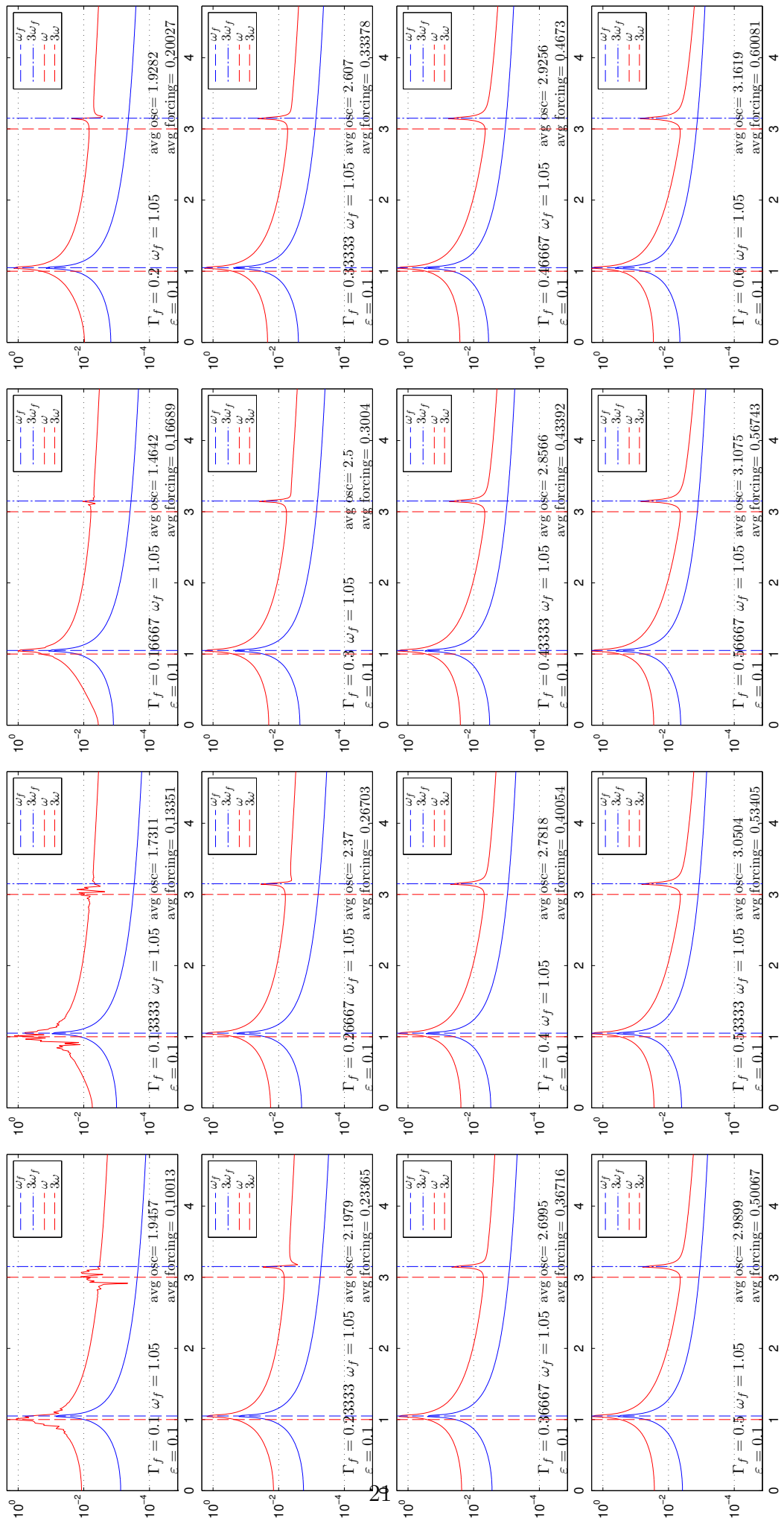


Figure 1.7: Spectrum of a VdP subject to increasing values of harmonic forcing at frequency  $\omega_f = 1.05$

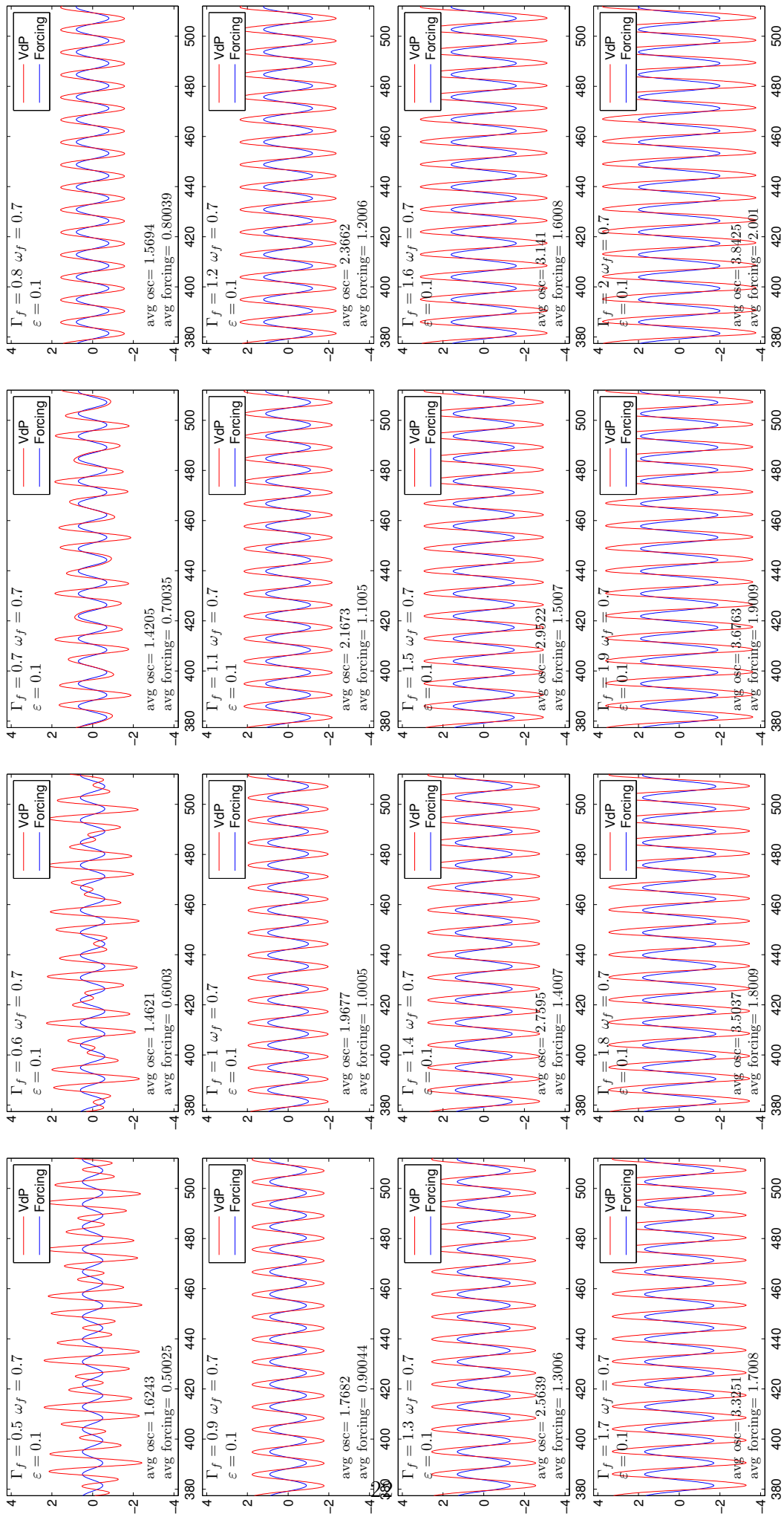


Figure 1.8: Time series of a VdP subject to increasing values of harmonic forcing at frequency  $\omega_f = 0.7$

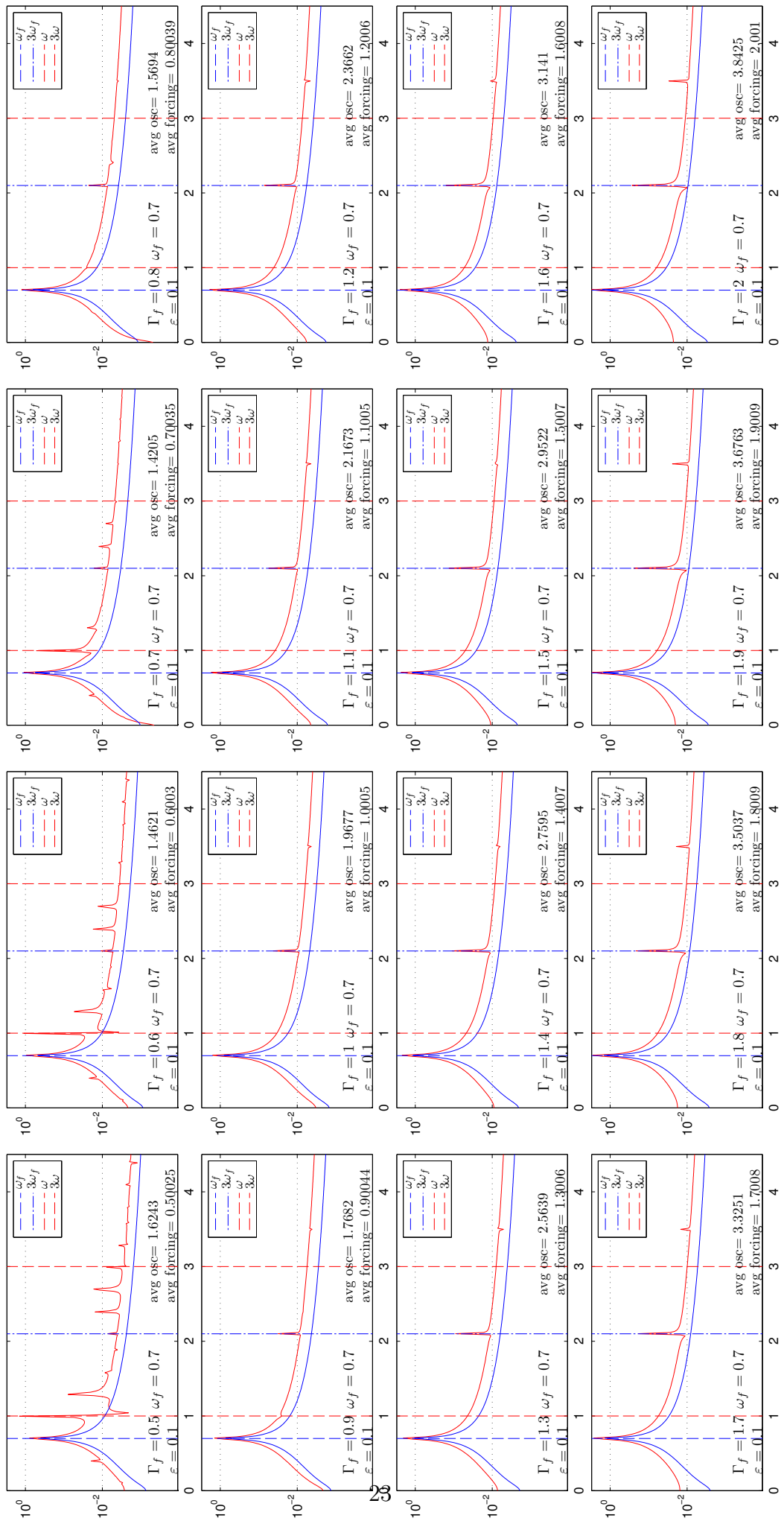


Figure 1.9: Spectrum of a VdP subject to increasing values of harmonic forcing at frequency  $\omega_f = 0.7$

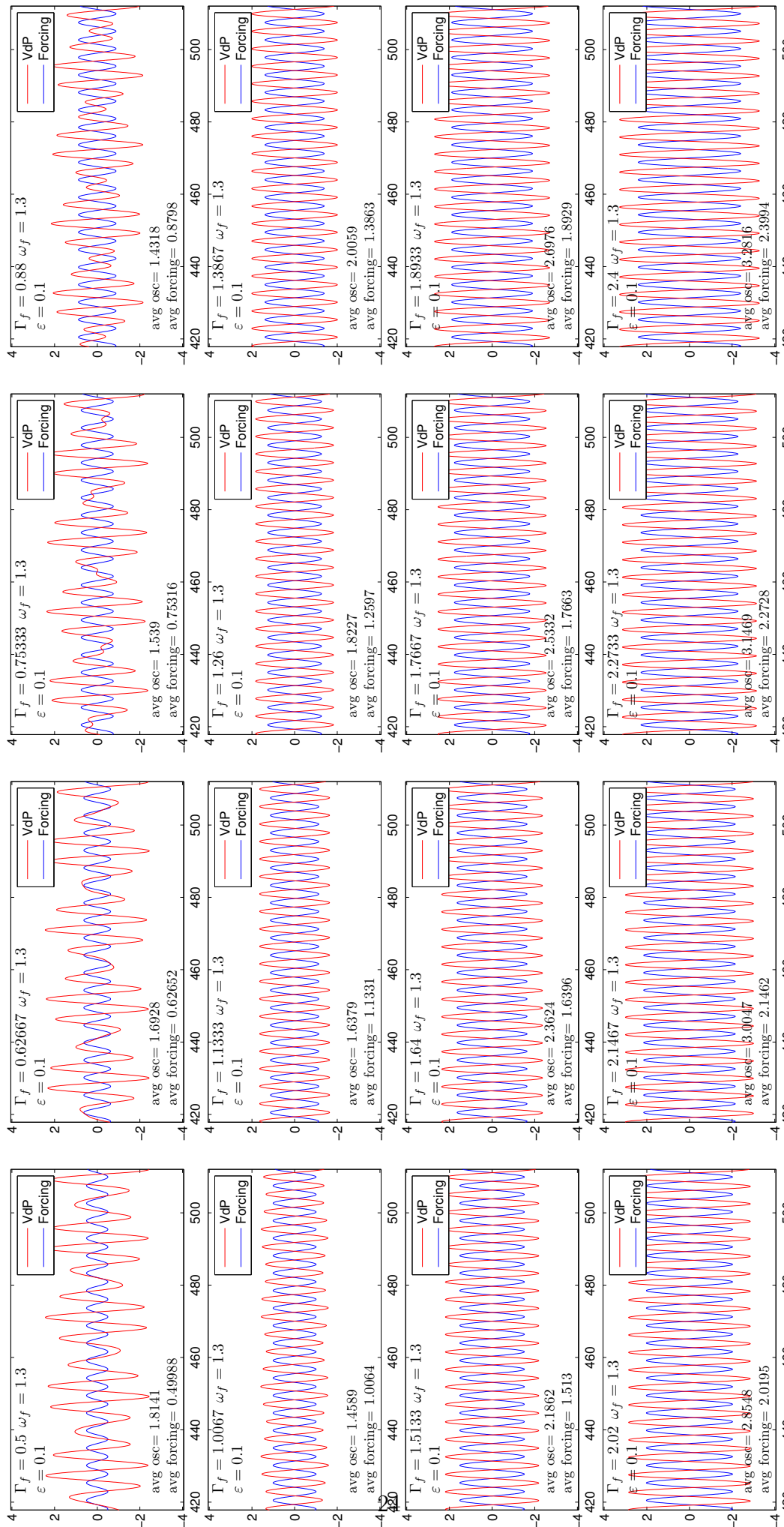


Figure 1.10: Time series of a VdP subject to increasing values of harmonic forcing at frequency  $\omega_f = 1.3$

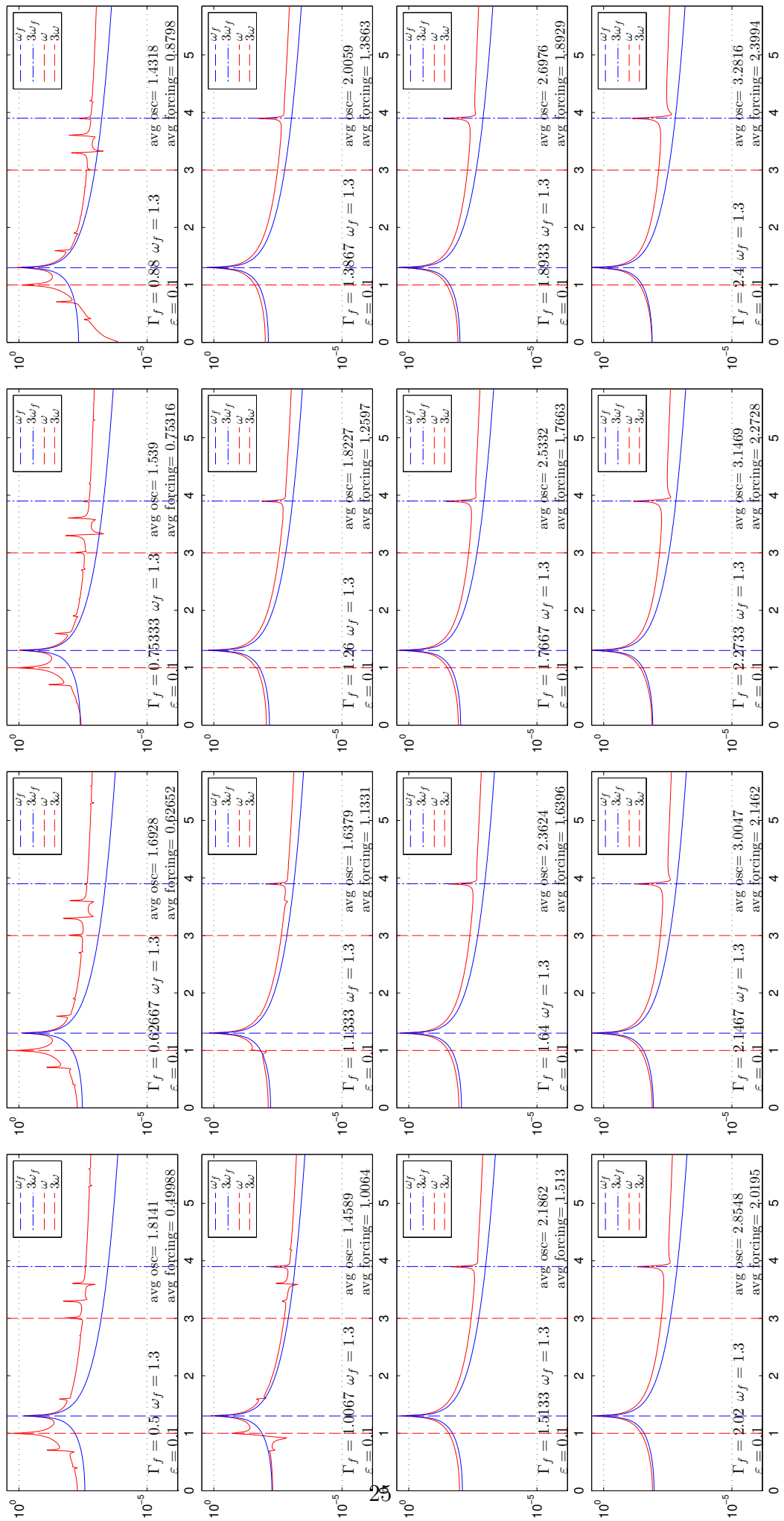


Figure 1.11: Spectrum of a VdP subject to increasing values of harmonic forcing at frequency  $\omega_f = 1.3$

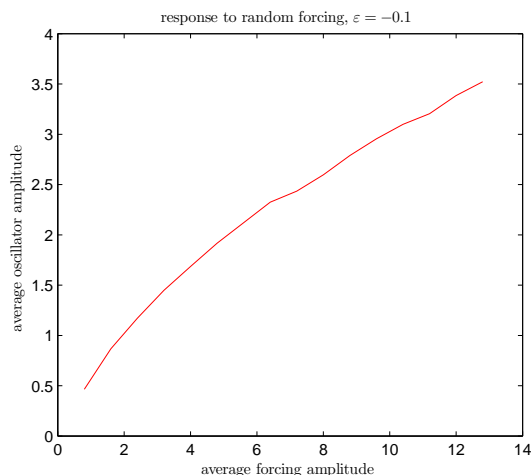


Figure 1.12: Final amplitude of a VdP subject to random forcing

## 1.4.2 Random forcing

Since we are investigating oscillators at the onset of their instability, we consider the behavior of a weakly stable oscillator fed by random noise. We observe that, above a certain threshold of the forcing intensity, the VdP begins oscillating at its natural frequency, with cycles disturbed by the non coherent nature of the forcing. In other terms, a weakly stable VdP fed by noise behaves like an unstable VdP plus some noise.

This scenario has a strong parallelism with a pocket of weakly absolutely stable flow. Typically, before this region becomes absolutely unstable, it is invested by convectively unstable perturbations developed upstream of the pocket. A promising development of this investigation is the modelling of this phenomenon as a VdP oscillator fed by noise with the same spectra of the perturbations coming from upstream.

In figure 1.13 and 1.14, we present the final state of a VdP fed by random noise, for increasing values of the forcing. The average of the signals is

$$\overline{a(t)} = \frac{\pi}{2T} \int_0^T |a(t)| dt, \quad (1.46)$$

where the factor  $\pi/2$  is such that the average of a sinusoidal function tends to 1 as  $T \rightarrow \infty$ . The system acts as a filter in the Fourier domain, and is slightly more sensitive to small forcing, as reported in figure 1.12.

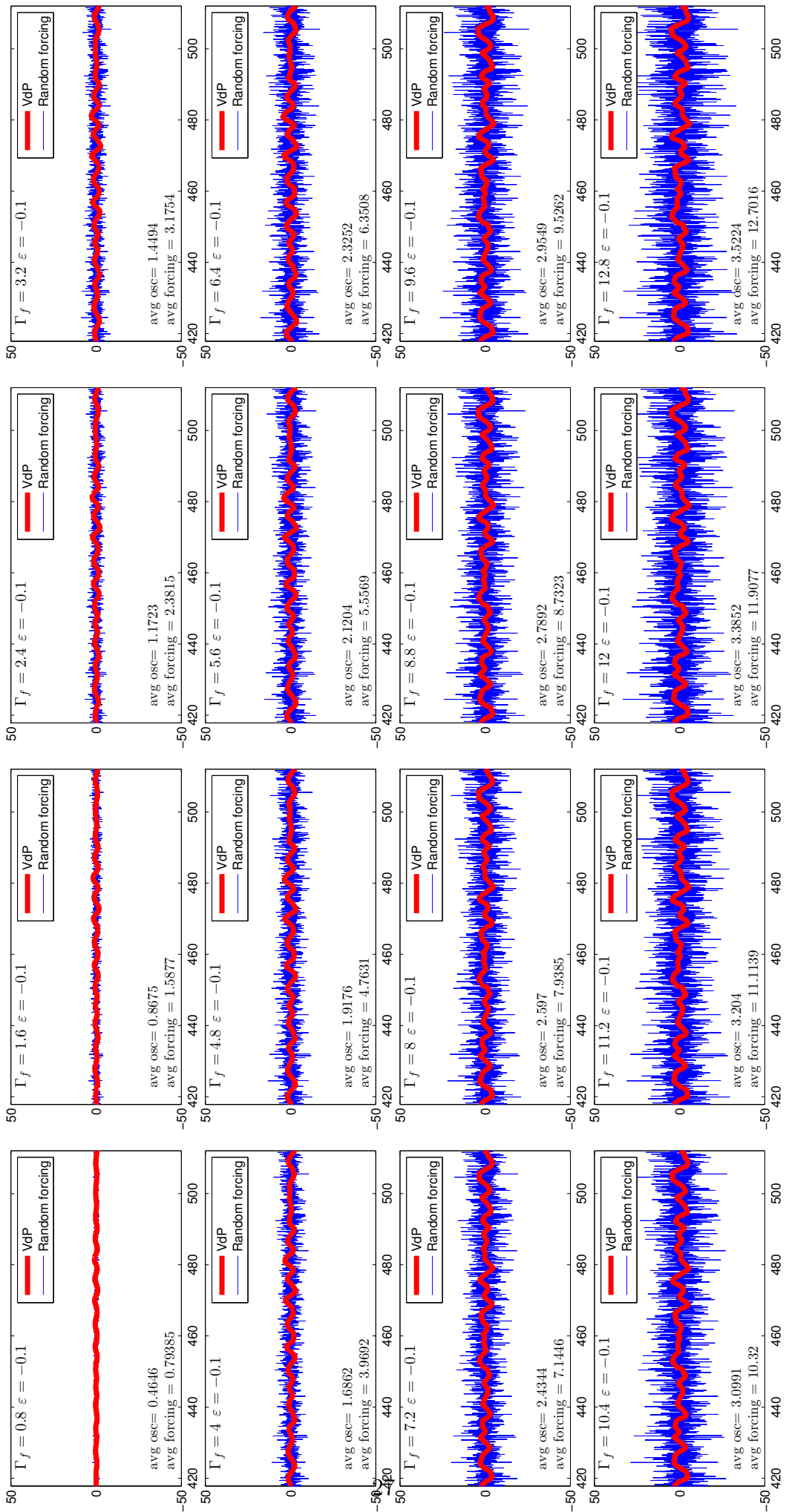


Figure 1.13: Time series of a VdP subject to increasing values of random forcing

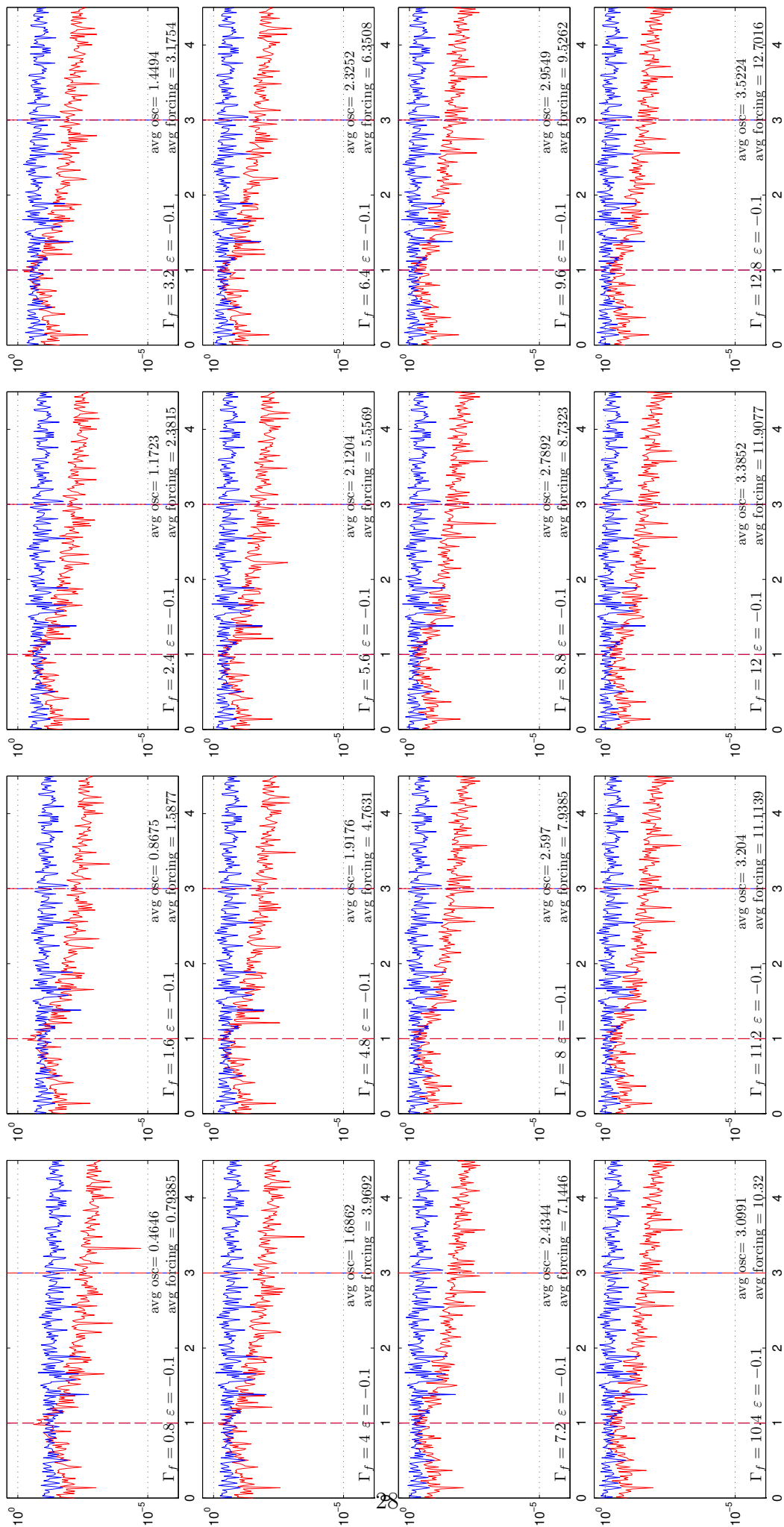


Figure 1.14: Fourier series of a VdP subject to increasing values of random forcing

# Chapter 2

## Coupled Van der Pol oscillators

### 2.1 The model

In the following we will consider a model expressing the features we want to describe and study in physics, and then manipulate the system to reduce the number of parameters and study it.

We choose a linear coupling between the two oscillators to keep the model as simple as possible. Since we want to apply these models to real phenomena, we begin allowing each of the oscillators to present its own limit-cycle amplitude  $A_i$  and angular frequencies  $\omega_i$ :

$$\begin{cases} \ddot{x}_1 + \varepsilon_1 \left( \operatorname{sgn}(\varepsilon_1) \frac{x_1^2}{A_1^2/4} - 1 \right) \omega_1 \dot{x}_1 \omega_1^2 x_1 &= \xi_{11} x_2 + \xi_{12} \omega_2 \dot{x}_2 \\ \ddot{x}_2 + \varepsilon_2 \left( \operatorname{sgn}(\varepsilon_2) \frac{x_2^2}{A_2^2/4} - 1 \right) \omega_2 \dot{x}_2 \omega_2^2 x_2 &= \xi_{22} x_1 + \xi_{21} \omega_1 \dot{x}_1 \end{cases} \quad (2.1)$$

$$x_j(0) = x_{0j} \quad \dot{x}_j(0) = \dot{x}_{0j} \quad j = 1, 2 \quad (2.2)$$

On the right of equations (2.1) we have the coupling terms between the two systems. This type of setup, where the coupling term of an oscillator is proportional to the amplitude of the other, is usually called direct coupling [1]. The coefficient  $\xi_{12}$  tunes how strong is the influence of the second oscillator on the first, the converse true for  $\xi_{21}$ . We manipulate algebraically the system to reduce the number of parameters involved, introducing

$$x_i(t) = A_i x_i(t)/2 \quad i = 1, 2. \quad (2.3)$$

Substituting (2.3) in (2.1), and defining

$$\mu_{1j} = \frac{\xi_{1j}A_2}{A_1}, \quad \mu_{2j} = \frac{\xi_{2j}A_1}{A_2}, \quad x_{0j} = 2x_{0j}/A_j, \quad \dot{x}_{0j} = 2\dot{x}_{0j}/A_j, \quad (2.4)$$

we obtain the new problem

$$\begin{cases} \ddot{x}_1 + \varepsilon_1(\operatorname{sgn}(\varepsilon_1)x_1^2 - 1)\omega_1\dot{x}_1 + \omega_1^2x_1 &= \mu_{11}x_2 + \mu_{12}\omega_2\dot{x}_2 \\ \ddot{x}_2 + \varepsilon_2(\operatorname{sgn}(\varepsilon_2)x_2^2 - 1)\omega_2\dot{x}_2 + \omega_2^2x_2 &= \mu_{22}x_1 + \mu_{21}\omega_1\dot{x}_1 \end{cases} \quad (2.5)$$

$$x_j(0) = x_{0j} \quad \dot{x}_j(0) = \dot{x}_{0j} \quad j = 1, 2 \quad (2.6)$$

We now study the problem in the new time variable  $\tau = t/\omega_1$ , in such a way that

$$(\dot{u}) \equiv (\dot{u})_\tau = \frac{1}{\omega_1}(\dot{u})_t. \quad (2.7)$$

Introducing  $\omega = \omega_2/\omega_1$ , and applying the chain derivation rule (2.7) in (2.5),

$$\begin{cases} \ddot{x}_1 + \varepsilon_1(\operatorname{sgn}(\varepsilon_1)x_1^2 - 1)\dot{x}_1 + x_1 &= \mu_{11}x_2 + \mu_{12}\omega\dot{x}_2 \\ \ddot{x}_2 + \varepsilon_2(\operatorname{sgn}(\varepsilon_2)x_2^2 - 1)\omega\dot{x}_2 + \omega^2x_2 &= \mu_{22}x_1 + \mu_{21}\dot{x}_1 \end{cases} \quad (2.8)$$

$$x_j(0) = x_{0j} \quad \dot{x}_j(0) = \omega_1\dot{x}_{0j} \quad j = 1, 2 \quad (2.9)$$

The two systems (2.8,2.9) and (2.1,2.2) are equivalent, and are linked by the definitions in (2.4), in such a way that

$$x_i(t) = A_i x_i(\omega_1 t)/2 \quad i = 1, 2. \quad (2.10)$$

The model (2.8,2.9) presents now seven parameters instead of ten, namely  $(\mu_{ij}, \omega, \varepsilon_j)$ .

We have already discussed how the nonlinear term  $\varepsilon$  for the single VdP had to be chosen small. For similar reasons, we will fix  $\varepsilon_j = 0.01$  in the following, further reducing the parameters to five.

## 2.2 Linear analysis

We now consider the linear version of (2.8), and rewrite it as a first-order system,

$$\dot{\mathbf{x}} = \mathbf{f}(\mathbf{x}), \quad \mathbf{x} = (x_1, y_1 := \dot{x}_1, x_2, y_2 := \dot{x}_2), \quad (2.11)$$

$$\begin{cases} \dot{x}_1 &= y_1 \\ \dot{y}_1 &= -x_1 + \varepsilon_1 y_1 + \omega \mu_{12} y_2 + \mu_{11} x_2 \\ \dot{x}_2 &= y_2 \\ \dot{y}_2 &= -\omega^2 x_2 + \omega \varepsilon_2 y_2 + \mu_{21} y_1 + \mu_{22} x_1 \end{cases} \quad (2.12)$$

This system presents a single fixed point at the origin. We study the eigenvalues  $\lambda$  of the Hessian  $\mathbf{H}(\mathbf{x}) = \nabla \mathbf{f}(\mathbf{x})$  calculated at the fixed point, solving the fourth-order equation

$$P(\lambda) = \det(\mathbf{H}(\mathbf{0}) - \lambda \mathbf{I}) = 0 \quad (2.13)$$

$$\begin{vmatrix} -\lambda & 1 & 0 & 0 \\ -1 & \varepsilon_1 - \lambda & \mu_{11} & \mu_{12}\omega \\ 0 & 0 & -\lambda & 1 \\ \mu_{22} & \mu_{21} & -\omega^2 & \varepsilon_2\omega - \lambda \end{vmatrix} = 0 \quad (2.14)$$

Developing the determinant, we study the solutions of

$$P(\lambda) = F_0 \lambda^4 + F_1 \lambda^3 + F_2 \lambda^2 + F_3 \lambda + F_4 = 0. \quad (2.15)$$

We are interested in the solution  $\lambda^*$  with the greatest real part, since it describes the less stable linear mode of the system. In particular, let

$$\lambda^* = \sigma + i\omega_{gl}, \quad (2.16)$$

where  $\sigma$  is the growth-rate, and  $\omega_{gl}$  is the linear global frequency, both real numbers. The coefficients of the polynomial  $P$  depend on the parameters of the

model:

$$\begin{cases} F_0 = 1 \\ F_1 = -\varepsilon_2\omega - \varepsilon_1 \\ F_2 = 1 + \omega^2 + \varepsilon_1\varepsilon_2\omega - \mu_{12}\mu_{21}\omega \\ F_3 = -\varepsilon_1\omega^2 - \varepsilon_2\omega - \mu_{12}\mu_{22}\omega - \mu_{11}\mu_{21} \\ F_4 = +\omega^2 - \mu_{11}\mu_{22} \end{cases} \quad (2.17)$$

Interestingly,

- for velocity coupling only, i.e. when  $\mu_{11} = \mu_{22} = 0$ , the linear stability problem depends only on the product  $\mu_{12}\mu_{21}$ .
- for displacement coupling only, i.e. when  $\mu_{12} = \mu_{21} = 0$ , the linear stability problem depends only on the product  $\mu_{11}\mu_{22}$ .

We can evaluate the stability of the system by determining if there exists at least one root with positive real part, applying the Routh-Hurwitz stability criterion. This involves verifying some inequalities involving the coefficients  $F_i$  presented in (2.17). Unfortunately, these expressions are not easy to tackle, and do not present an easily understandable picture of the stability.

**Approximate stability criterion** We consider now  $\varepsilon_i$  negligible, and calculate the analytical solution for the two cases of velocity and displacement coupling. For velocity coupling, setting  $k \equiv \mu_{12}\mu_{21}$ ,

$$P(\lambda) = \lambda^4 + (1 + \omega^2 - k\omega)\lambda^2 + \omega^2 = 0 \quad (2.18)$$

$$\lambda^2 = \frac{1}{2} \left[ (k\omega - (1 + \omega^2)) \pm \sqrt{(k\omega - (1 + \omega^2))^2 - 4\omega^2} \right] \quad (2.19)$$

$$= \frac{1}{2} (b \pm \sqrt{a}) \quad (2.20)$$

Since the discriminant  $a$  is always smaller than  $b^2$ , the real part of  $\lambda^2$  is positive only if  $b$  is positive. Then, the system is unstable only if  $b > 0$ , i.e. if

$$k > \frac{1 + \omega^2}{\omega} \quad (2.21)$$

For displacement coupling, we have

$$P(\lambda) = \lambda^4 + (1 + \omega^2)\lambda^2 + (\omega^2 - k) = 0 \quad (2.22)$$

$$\lambda^2 = \frac{1}{2} \left[ -(1 + \omega^2) \pm \sqrt{(1 - \omega^2)^2 + 4k} \right] \quad (2.23)$$

and the system is unstable for

$$4k > \omega^2 \quad (2.24)$$

### 2.2.1 Effect of the coupling on the stability

In this section we show that two coupled, stable oscillators can become unstable due to the coupling. We discuss here some of the results presented by Al Qadri et al. [6]. They run two global stability analyses of two subdomains of the flow, in correspondence of two distinct pockets of slightly absolutely stable flow. We will refer to the two as bubble/oscillator 1 and wake/oscillator 2. Their linear properties are

$$\begin{cases} \omega_{l1} = 1.0640 \\ \sigma_{l1} = -0.0035 \end{cases} \quad \begin{cases} \omega_{l2} = 0.9675 \\ \sigma_{l2} = -0.0935 \end{cases} \quad (2.25)$$

We tune the single oscillators as explained in section 1.3. [6] also did the stability analysis of the whole domain, that corresponds to the coupled system, observing that the the whole domain is unstable. They calculate these linear properties:

$$\begin{cases} \omega_{gl} = 1.0655 \\ \sigma_{gl} = 0.0005 \end{cases} \quad (2.26)$$

We then study the stability of the system in the case of velocity and displacement coupling, parametrically in  $\kappa$ . In figure 2.1.a and 2.1.b we report the real part  $\sigma$  and the imaginary part  $\omega$  of the two conjugated pairs solutions of the system (2.15), in the case of velocity and displacement coupling. We evaluate the critical value of  $\kappa$  that leads to instability, i.e. such that one of the two solutions presents  $\sigma = 0$ , and the value that matches the global behavior,  $\sigma = \sigma_{gl}$ .

In figure 2.1.c we consider a particular coupling, setting  $\mu_{22} = \alpha\mu_{21}, \mu_{11} = \alpha\mu_{12}$ , with  $\alpha = 1.55$ . For this configuration, we match both the growth-rate

and the global frequency of the global mode described by (2.26). This suggests that given the six parameters  $\omega_{l1}, \omega_{l2}, \sigma_{l1}, \sigma_{l2}, \omega_{gl}\sigma_{gl}$ , it may be possible to tune the coupling coefficients to get a coupled system that presents these six linear properties.

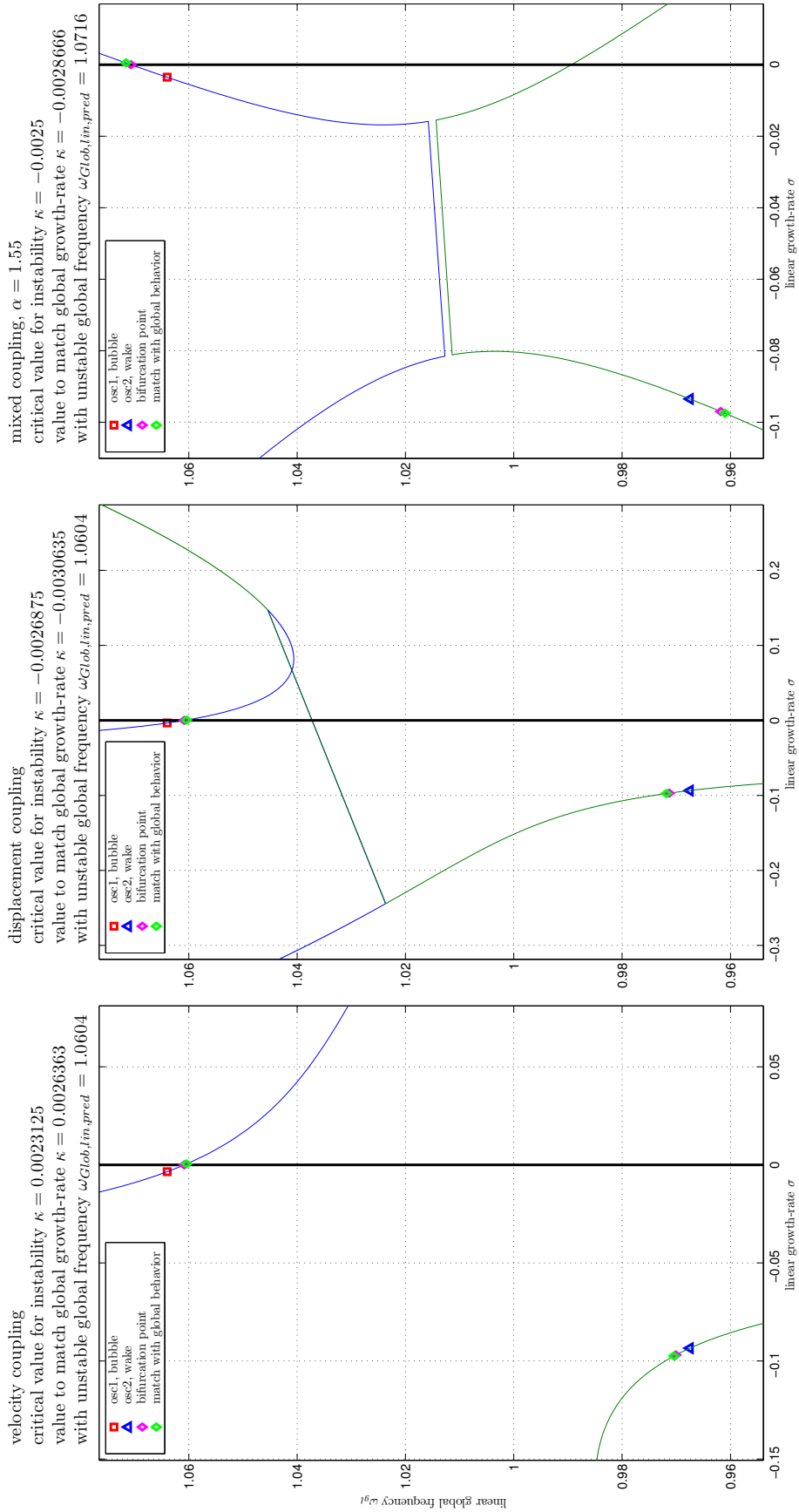


Figure 2.1: Linear stability analysis of the coupled system, as a function of  $\kappa$ . For  $\kappa = 0$ , the analysis coincides with the parameters presented in (2.25). The analysis on the right presents a specific coupling such that the global frequency coincides with the given value of  $\omega_{gl}$  in (2.26)

## 2.3 Introductory simulation results

In this section we discuss a limited set of simulations of the coupled system, discussing part of its behavior in a qualitative way. This is a required step, because part of the theoretical results obtained in the next sections are founded on some experimental features of the system. We are interested in the time and Fourier series of the system (2.8) after the initial transient in time, that is dependent on the initial conditions (2.9). In this first array of simulations, all the  $\mu_{ij}$  dots stand on a same line in their four-dimensional space, that crosses the origin. I have chosen a line far from each of the 4 axes in the coupling space, since close to each of them one of the two oscillators is entrained to the other and doesn't influence it, as discussed in the section 1.4.1. To this aim, I have chosen:

$$\begin{cases} \mu_{12} = d \cos \alpha \\ \mu_{21} = d \sin \alpha \\ \mu_{11} = d \cos \alpha \\ \mu_{22} = d \sin \alpha \end{cases} \quad \begin{cases} \alpha = -\pi/6 \\ d \in [0 \ 4] \end{cases} \quad (2.27)$$

In these two figures, from left to right and from top to bottom, we are considering an increasing distance  $\bar{\mu}$ , defined as

$$\bar{\mu} \equiv \sqrt{\mu_{11}^2 + \mu_{12}^2 + \mu_{22}^2 + \mu_{21}^2}. \quad (2.28)$$

In figure 2.2 and 2.3 we report the simulations for values of  $\bar{\mu}$  linearly spaced between 0.01 and 0.4. In both figures we can observe in the first two top left simulations quasi periodic solution, with average oscillations close to 2, the natural limit-cycle oscillation of a single VdP.

Than the coupling becomes strong enough to entrain the two oscillators to a common global frequency  $\omega_g$ . The horizontal lines in figure 2.2 show the predicted values of the limit-cycle amplitudes using the averaging method, that will be illustrated in section 2.4. The vertical green line in figure 2.2 is the global frequency as predicted by the same method.

We then consider a stronger coupling  $\bar{\mu}$ , in the interval [0.4 4], in figures 2.4 and 2.5. The global frequency significantly drifts away from the two natural frequencies. This is interesting, but it is not a general result, and  $\omega$  can grow or

decrease with  $\bar{\mu}$ . This depends on the inclination of the vector of the parameters  $\{\mu_{ij}\}$  in their four-dimensional space, and on the phase lag between the two solutions. On the other hand, this is a linear phenomena, due to the growth of the coupling, and only secondarily a nonlinear one.

Observe how higher-order harmonics become larger compared to the first harmonic. This happens because for larger values of  $\bar{\mu}$  the amplitude of the oscillators grows, and the nonlinear term  $\dot{x}x^2$  in each oscillator grows more than the other terms, that are all linear. In turn, the nonlinear term is the source of higher harmonics.

The limit-cycle amplitudes that accompany these strong high-order harmonics are much larger than the limit-cycle amplitude of a single VdP, that is 2. When studying the interaction between stable/unstable modes, it is possible that, for the purpose of the model, the required value of  $\bar{\mu}$  may stay well below 0.5. For this reason, we will restrict the scope of this investigation for values of  $\bar{\mu}$  below this value.

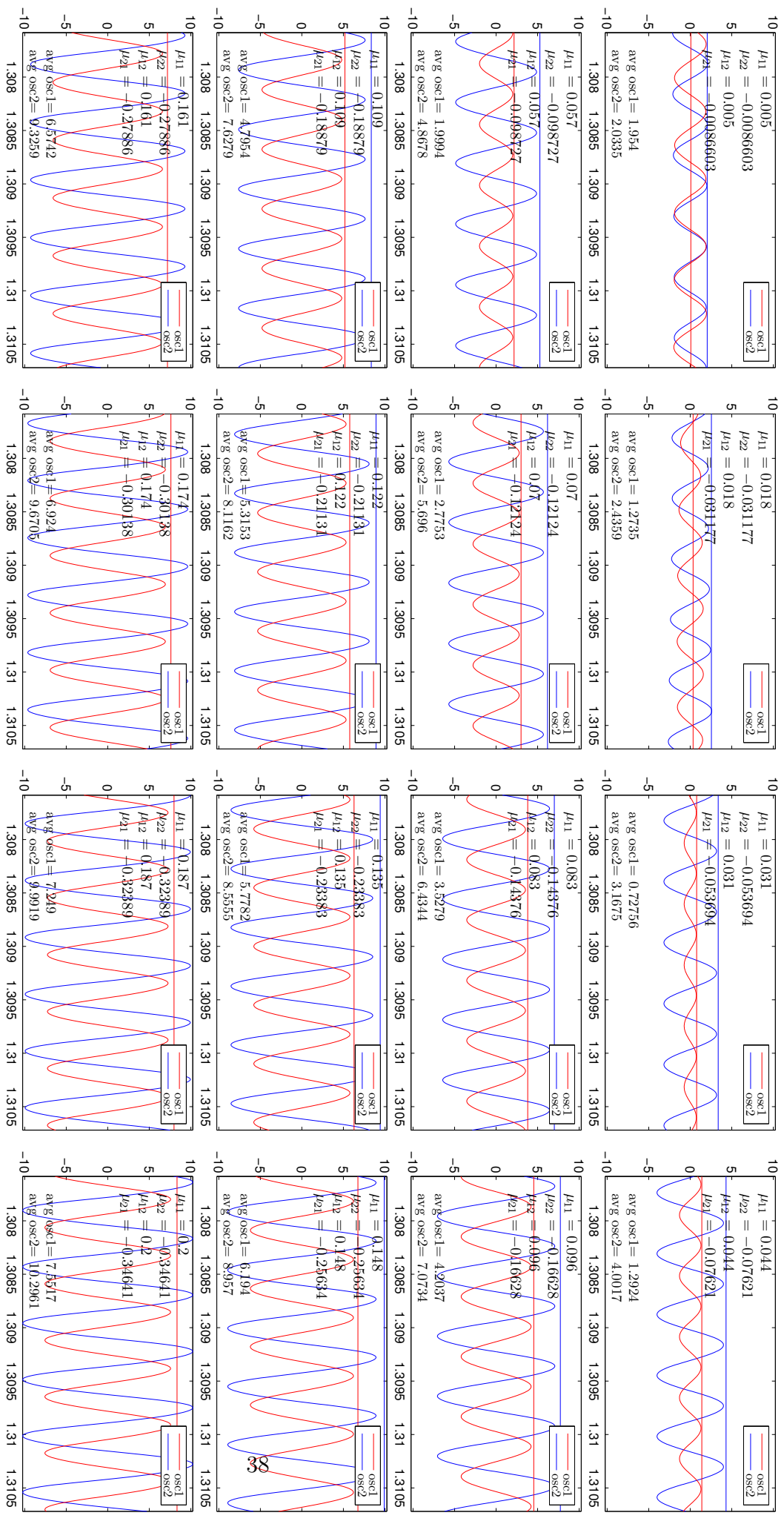


Figure 2.2: Time series of two coupled VDP subject to increasing values of coupling, between 0.01 and 0.4. The ratio of the second oscillator's natural frequency to the first's is  $\omega = 1.1$

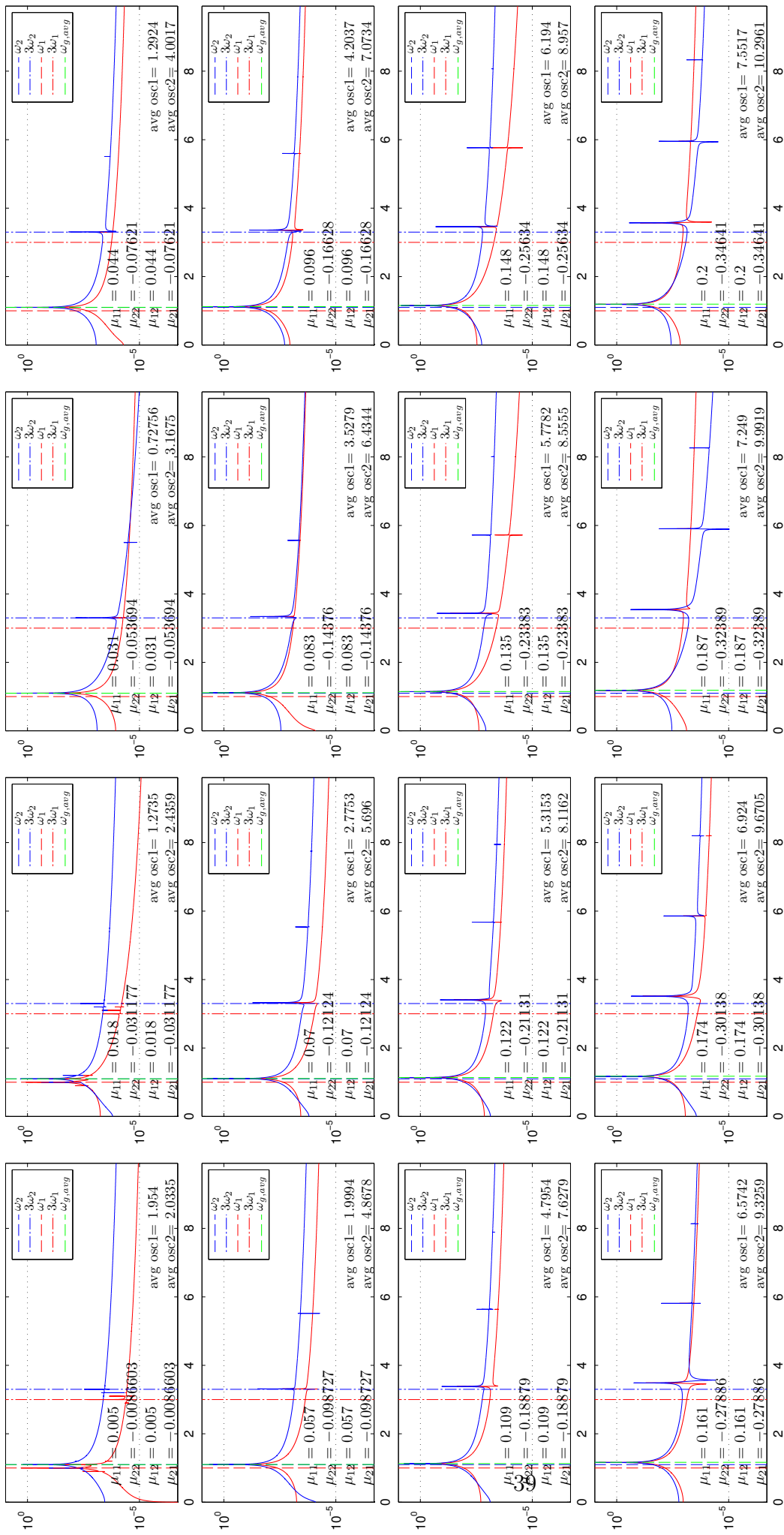


Figure 2.3: Fourier series of two coupled VdP subject to increasing values of coupling, between 0.01 and 0.4. The ratio of the second oscillator's natural frequency to the first's is  $\omega = 1.1$

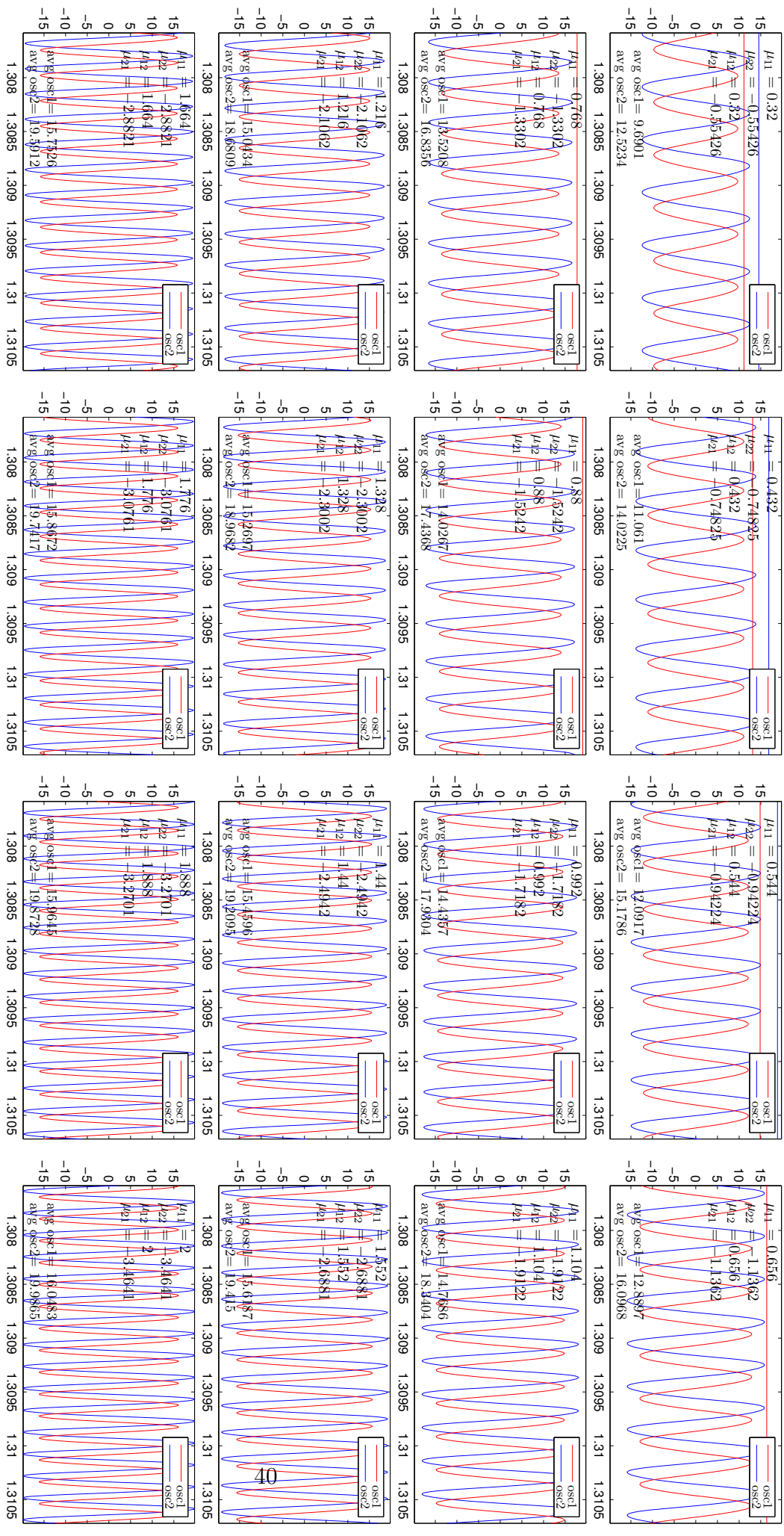


Figure 2.4: Time series of two coupled VdP subject to increasing values of coupling. The ratio of the second oscillator's natural frequency to the first's is  $\omega = 1.1$

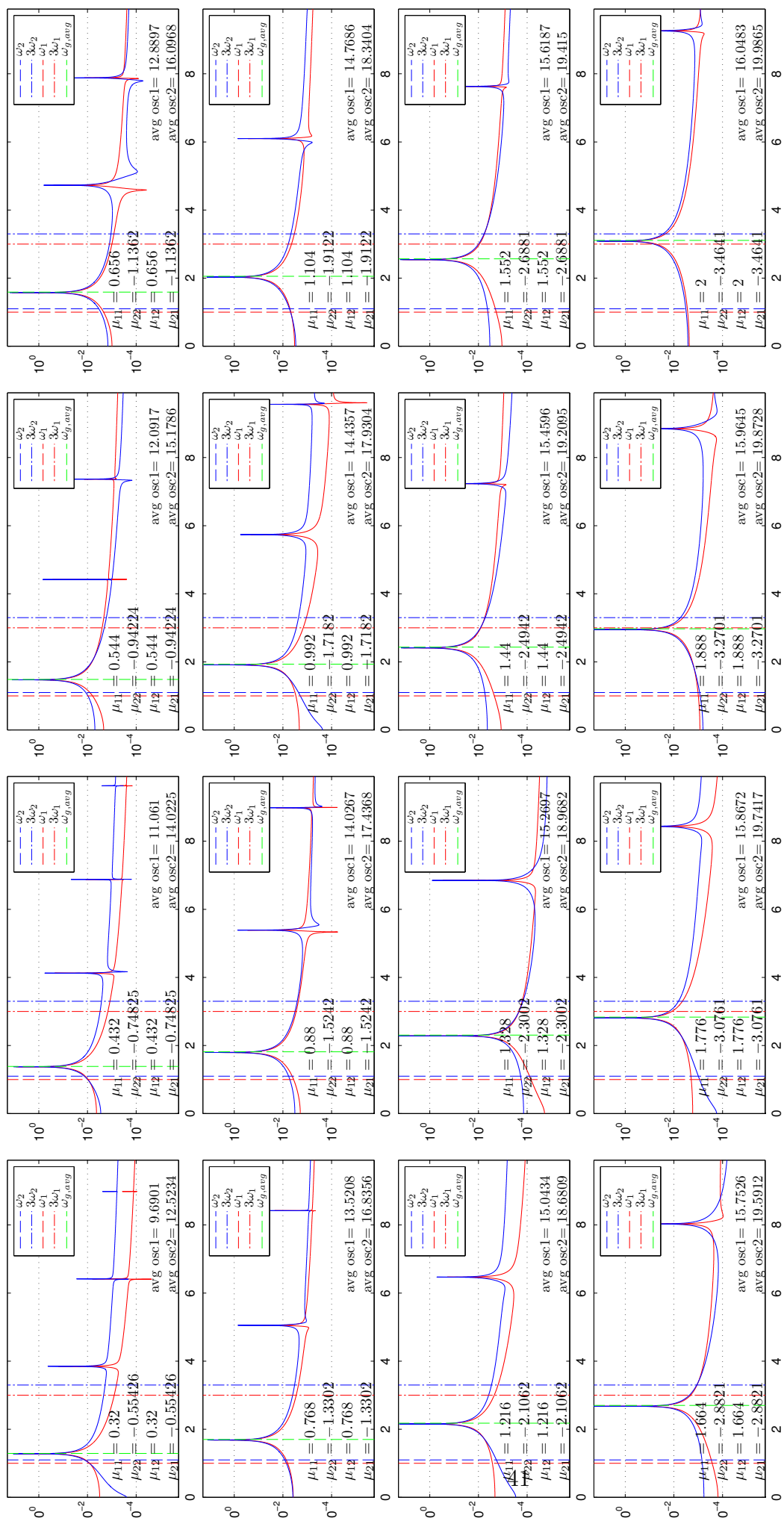


Figure 2.5: Fourier series of two coupled VdP subject to increasing values of coupling. The ratio of the second oscillator's natural frequency to the first's is  $\omega = 1.1$

## 2.4 Method of averaging

We now reformulate the problem as a first order differential equation in the form (1.5),

$$\begin{aligned} \dot{\mathbf{x}} &= \mathbf{A}\mathbf{x} + \varepsilon \mathbf{f}^1(\mathbf{x}, t) & (2.29) \\ \begin{bmatrix} \dot{x}_1 \\ \dot{y}_1 \\ \dot{x}_2 \\ \dot{y}_2 \end{bmatrix} &= \begin{bmatrix} 0 & 1 & 0 & 0 \\ -1 & 0 & \mu_{11} & \mu_{12}\omega \\ 0 & 0 & 0 & 1 \\ \mu_{22} & \mu_{21} & -\omega^2 & 0 \end{bmatrix} \begin{bmatrix} x_1 \\ y_1 \\ x_2 \\ y_2 \end{bmatrix} + \varepsilon_1 \begin{bmatrix} 0 \\ -(\text{sgn}(\varepsilon_1)x_1^2 - 1)y_1 \\ 0 \\ -\frac{\varepsilon_2}{\varepsilon_1}(\text{sgn}(\varepsilon_2)x_2^2 - 1)\omega y_2 \end{bmatrix} & (2.30) \end{aligned}$$

In this expression, notice that the two linear terms  $\varepsilon_1 y_1$  and  $\varepsilon_2 \omega y_2$  were not included in the linear part  $\mathbf{A}\mathbf{x}$ , or in other words that  $\mathbf{A}\mathbf{x}$  is not the linear part of the problem. Their inclusion would lead to a solution of the zero-order system  $\dot{\mathbf{x}} = \mathbf{A}\mathbf{x}$ , either growing or decaying exponentially depending on the sign of  $\varepsilon$ ; this would lead to a slow flow respectively decaying or growing exponentially to contrast that behavior<sup>1</sup>.

We can't now calculate the exponential of the matrix  $\mathbf{A}$  that would lead to the solution of the unperturbed problem<sup>2</sup>. Two important considerations lead now to different approaches.

Firstly, we know that for large enough coupling we observe entrainment of the two VdP at a global nonlinear frequency  $\omega_g$ , as defined in 2.2. This is typical of systems subject to synchronization: if the coupling is strong enough, the oscillators start behaving as a single system [5]. In section 2.4.1 we will consider the two VdP oscillating at a common global frequency, and discuss that solution.

Secondly, we will investigate the scenario where the two VdP oscillate at their respective natural frequencies, in section 2.4.2. We are expecting this to work for small enough coupling.

---

<sup>1</sup>Assuming the solution to be bounded and not null in the limit of  $t \rightarrow \infty$ .

<sup>2</sup>Refer to the passage from equation (1.7) to equation (1.8)

## 2.4.1 Entrained Solution

We choose a solution

$$\begin{cases} x_1 = r_1 \sin(\omega_g t - \varphi_1) \equiv r_1 s_1 \\ y_1 = \omega_g r_1 \cos(\omega_g t - \varphi_1) \equiv \omega r_1 c_1 \\ x_2 = r_2 \sin(\omega_g t - \varphi_2) \equiv r_2 s_2 \\ y_2 = \omega_g r_2 \cos(\omega_g t - \varphi_2) \equiv \omega r_2 c_2 \end{cases}, \quad (2.31)$$

being  $r_i$  and  $\varphi_i$  functions of time. We proceed substituting in (2.30), obtaining

$$\dot{r}_1 s_1 - \dot{\varphi}_1 r_1 c_1 = 0 \quad (2.32)$$

$$\dot{r}_1 c_1 \omega_g - r_1 s_1 \omega_g^2 + r_1 s_1 \omega_g \dot{\varphi}_1 = -r_1 s_1 + \mu_{11} r_2 s_2 + \mu_{12} \omega r_2 c_2 \omega_g + \varepsilon_1 f_2^1 \quad (2.33)$$

$$\dot{r}_2 s_2 - \dot{\varphi}_2 r_2 c_2 = 0 \quad (2.34)$$

$$\dot{r}_2 c_2 \omega_g - r_2 s_2 \omega_g^2 + r_2 s_2 \omega_g \dot{\varphi}_2 = -r_2 s_2 \omega^2 + \mu_{22} r_1 s_1 + \mu_{21} r_1 c_1 \omega_g + \varepsilon_1 f_4^1 \quad (2.35)$$

Now, multiplying (2.32) by  $s_1 \omega_g$ , and adding it to (2.33) multiplied by  $c_1$ , we obtain

$$\dot{r}_1 \omega_g - r_1 c_1 s_1 \omega_g^2 = -r_1 c_1 s_1 + \mu_{11} r_2 c_1 s_2 + \mu_{12} \omega r_2 c_2 c_1 \omega_g + \varepsilon_1 f_2^1 c_1 \quad (2.36)$$

Similarly, multiplying (2.32) by  $c_1 \omega_g$ , and subtracting it to (2.33) multiplied by  $s_1$ , we obtain

$$-r_1 s_1^2 \omega_g^2 + \dot{\varphi}_1 r_1 \omega_g = -r_1 s_1^2 + \mu_{11} r_2 s_2 s_1 + \mu_{12} \omega \omega_g r_2 c_2 s_1 + \varepsilon_1 f_2^1 s_1 \quad (2.37)$$

In the same way, we obtain two expressions for  $\dot{r}_2$  and  $\dot{\varphi}_2$ . The four resulting equations are

$$\begin{cases} \dot{r}_1 \omega_g = r_1 c_1 s_1 (\omega_g^2 - 1) + \mu_{11} r_2 c_1 s_2 + \mu_{12} \omega r_2 c_2 c_1 \omega_g + \varepsilon_1 f_2^1 c_1 \\ \dot{r}_2 \omega_g = r_2 c_2 s_2 (\omega_g^2 - \omega^2) + \mu_{22} r_1 c_2 s_1 + \mu_{21} r_1 c_2 c_1 \omega_g + \varepsilon_1 f_4^1 c_2 \\ \dot{\varphi}_1 \omega_g = s_1^2 (\omega_g^2 - 1) + \mu_{11} \frac{r_2}{r_1} s_2 s_1 + \mu_{12} \omega \omega_g \frac{r_2}{r_1} c_2 s_1 + \frac{\varepsilon_1}{r_1} f_2^1 s_1 \\ \dot{\varphi}_2 \omega_g = s_2^2 (\omega_g^2 - \omega^2) + \mu_{22} \frac{r_1}{r_2} s_2 s_1 + \mu_{21} \omega_g \frac{r_1}{r_2} c_1 s_2 + \frac{\varepsilon_1}{r_2} f_4^1 s_2 \end{cases} \quad (2.38)$$

We now apply the method of averaging, calculating the average of the RHS in a period  $T = 2\pi/\omega_g$ . The reader may observe that the system (2.38) is not in the standard form (1.20), since a few terms are  $O(1)$  instead of all being  $O(\varepsilon)$ . Applying the average operator<sup>3</sup> defined in (1.23), we observe that:

- the factors of  $c_i s_i$  disappear, since  $\overline{s_i c_i} = 0$ .
- the averages of products of even powers of the sin and cos functions are non-zero,

$$\overline{c_i^2} = \overline{s_i^2} = \frac{1}{T} \int_{-T/2}^{T/2} \sin^2 u du = \frac{1}{2}; \quad \overline{c_i^2 s_i^2} = \frac{1}{8} \quad (2.39)$$

- mixed terms like  $s_1 c_2$  require a different treatment,

$$\begin{aligned} \overline{s_1 c_2} &= \frac{\omega_g}{2\pi} \int_{-\pi/\omega_g}^{\pi/\omega_g} \sin(\omega_g t - \varphi_1) \cos(\omega_g t - \varphi_2) dt \\ &= \frac{1}{2\pi} \int_{-\pi}^{\pi} \sin(v) \cos(v + (\varphi_1 - \varphi_2)) dv \\ &= \frac{\cos(\varphi_1 - \varphi_2)}{2\pi} \int_{-\pi}^{\pi} \sin v \cos v dv - \frac{\sin(\varphi_1 - \varphi_2)}{2\pi} \int_{-\pi}^{\pi} \sin^2 v dv \\ &= -s_\theta/2, \end{aligned} \quad (2.40)$$

where we have introduced the instantaneous phase lag

$$\theta(t) = \varphi_1(t) - \varphi_2(t), \quad (2.41)$$

and employed the notation  $s_\theta \equiv \sin \theta$ ,  $c_\theta \equiv \cos \theta$ .

Operating in a similar way, we obtain

$$\overline{s_2 c_1} = s_\theta/2 \quad \overline{c_1 c_2} = \overline{s_1 s_2} = c_\theta/2 \quad (2.42)$$

---

<sup>3</sup>We recall that the method approximates the solution considering the variables  $\varphi_i, r_i$  to be not function of time in the averaging integral

Averaging the linear terms in the system (2.38), we obtain:

$$\begin{cases} \dot{r}_1 \omega_g &= (s_\theta \mu_{11} + c_\theta \mu_{12} \omega \omega_g) \frac{r_2}{2} + \varepsilon_1 \overline{f_2^1 c_1} \\ \dot{r}_2 \omega_g &= (c_\theta \mu_{21} \omega_g - s_\theta \mu_{22}) \frac{r_1}{2} + \varepsilon_1 \overline{f_4^1 c_2} \\ \dot{\varphi}_1 \omega_g &= \frac{1}{2}(\omega_g^2 - 1) + (c_\theta \mu_{11} - s_\theta \mu_{12} \omega \omega_g) \frac{r_2}{2r_1} + \varepsilon_1 \overline{f_2^1 s_1} / r_1 \\ \dot{\varphi}_2 \omega_g &= \frac{1}{2}(\omega_g^2 - \omega^2) + (c_\theta \mu_{22} + \mu_{21} \omega_g s_\theta) \frac{r_1}{2r_2} + \varepsilon_1 \overline{f_4^1 s_2} / r_2 \end{cases} \quad (2.43)$$

The average of the nonlinear terms:

$$\begin{aligned} \overline{f_2^1 c} &= -\operatorname{sgn}(\varepsilon_1) \frac{1}{8} r_1^3 + \frac{1}{2} r_1 = \frac{r_1}{2} \left[ 1 - \operatorname{sgn}(\varepsilon_1) \left( \frac{r_1}{2} \right)^2 \right] \\ \overline{f_4^1 c} &= \frac{\varepsilon_2}{\varepsilon_1} \left[ -\operatorname{sgn}(\varepsilon_2) \frac{1}{8} r_2^3 + \frac{1}{2} r_2 \right] = \frac{\varepsilon_2}{\varepsilon_1} \frac{r_2}{2} \left[ 1 - \operatorname{sgn}(\varepsilon_2) \left( \frac{r_2}{2} \right)^2 \right] \\ \overline{f_2^1 s} &= \overline{f_4^1 s} = 0 \end{aligned} \quad (2.44)$$

Substituting equations (2.44) in (2.43), we obtain the slow flow equations<sup>4</sup>:

$$\begin{aligned} \dot{\bar{\zeta}} &= \bar{\mathbf{g}}(\bar{\zeta}, \varepsilon, t) = \bar{\mathbf{g}}_1(\bar{\zeta}, t) + \varepsilon \bar{\mathbf{g}}_\varepsilon(\bar{\zeta}, t) \\ \begin{cases} \dot{r}_1 \omega_g &= (s_\theta \mu_{11} + c_\theta \mu_{12} \omega \omega_g) \frac{r_2}{2} + \varepsilon_1 \frac{r_1}{2} - |\varepsilon_1| \left( \frac{r_1}{2} \right)^3 \\ \dot{r}_2 \omega_g &= (c_\theta \mu_{21} \omega_g - s_\theta \mu_{22}) \frac{r_1}{2} + \varepsilon_2 \frac{r_2}{2} - |\varepsilon_2| \left( \frac{r_2}{2} \right)^3 \\ \dot{\varphi}_1 \omega_g &= \frac{1}{2}(\omega_g^2 - 1) + (c_\theta \mu_{11} - s_\theta \mu_{12} \omega \omega_g) \frac{r_2}{2r_1} \\ \dot{\varphi}_2 \omega_g &= \frac{1}{2}(\omega_g^2 - \omega^2) + (c_\theta \mu_{22} + \mu_{21} \omega_g s_\theta) \frac{r_1}{2r_2} \end{cases} \end{aligned} \quad (2.45)$$

We observe that the RHS of (2.45,2.46) contain terms that are  $O(1)$ , while the method of averaging as applied to a single VdP in section 1.2 lead to a system of the form (1.31), where all the RHS is  $O(\varepsilon)$ . In other words, the trial solution (2.31) is not, in general, the solution of the unperturbed problem, and then the outcome of the method of averaging presents, in general, the  $O(1)$  term  $\bar{\mathbf{g}}_1(\bar{\zeta}, t)$  appearing in (2.45).

The system (2.46) presents a symmetry with respect to the parameters, in particular if  $\zeta = (r_1, r_2, \theta, \omega_g)$  is solution for the set of parameters  $\{\mu_{ij}\}$ , then  $\zeta' = (r_1, r_2, \theta + \pi, \omega_g)$  is solution for the set of parameters  $\{-\mu_{ij}\}$ .

---

<sup>4</sup>Compare with equation (1.33)

We will now calculate the general solution of the system (2.45). It will be later discussed in 2.4.1.2 if this solution converges to the solution of the unperturbed problem for  $\varepsilon \rightarrow 0$ , as it happens for the VdP.

**Different formulation** It is possible to introduce  $\kappa_1, \alpha_1$  and  $\kappa_2, \alpha_2$ :

$$\begin{cases} \kappa_1 &= \sqrt{\mu_{11}^2 + (\mu_{12}\omega\omega_g)^2} \\ \alpha_1 &= \tan^{-1}\left(\frac{\mu_{11}}{\mu_{12}\omega\omega_g}\right) \end{cases} \text{ in such a way that } \begin{cases} \mu_{11} &= \kappa_1 s_{\alpha_1} \\ \mu_{12}\omega\omega_g &= \kappa_1 c_{\alpha_1} \end{cases} \quad (2.47)$$

$$\begin{cases} \kappa_2 &= \sqrt{\mu_{22}^2 + (\mu_{21}\omega_g)^2} \\ \alpha_2 &= \tan^{-1}\left(\frac{\mu_{22}}{\mu_{21}\omega_g}\right) \end{cases} \text{ in such a way that } \begin{cases} \mu_{22} &= \kappa_2 s_{\alpha_2} \\ \mu_{21}\omega_g &= \kappa_2 c_{\alpha_2} \end{cases} \quad (2.48)$$

Notice how this allows an understanding of the coupling via the  $(\kappa_i, \alpha_i)$  parameters instead of  $(\mu_{i1}, \mu_{i2})$ . Substituting these expressions in the system (2.46), we obtain

$$\begin{cases} \dot{r}_1\omega_g &= \kappa_1 \cos(\theta - \alpha_1)\frac{r_2}{2} + \varepsilon_1\frac{r_1}{2} - |\varepsilon_1|\left(\frac{r_1}{2}\right)^3 \\ \dot{r}_2\omega_g &= \kappa_2 \cos(\theta + \alpha_2)\frac{r_1}{2} + \varepsilon_2\frac{r_2}{2} - |\varepsilon_2|\left(\frac{r_2}{2}\right)^3 \\ \dot{\varphi}_1\omega_g &= \frac{1}{2}(\omega_g^2 - 1) + \kappa_1 \sin(\theta - \alpha_1)\frac{r_2}{2r_1} \\ \dot{\varphi}_2\omega_g &= \frac{1}{2}(\omega_g^2 - \omega^2) + \kappa_2 \sin(\theta + \alpha_2)\frac{r_1}{2r_2} \end{cases} \quad (2.49)$$

Unfortunately,  $\omega_g$  is in the definition of the new parameters, and this doesn't allow a simple tuning.

### 2.4.1.1 General solution

We want to discuss then the slow flow (2.46) with the  $O(\varepsilon)$  terms contrasting the  $O(1)$  terms. We look now for the conditions under which the slow flow in (2.46) presents a stable entrained solution, and determine the limit-cycle amplitudes of that case. The two oscillators are entrained if the phase lag  $\theta(t) = \varphi_1(t) - \varphi_2(t)$  is constant with time, i.e. if  $\dot{\theta} = 0$ . We also restrict our analysis to the case in which the entrained frequency doesn't vary with time, imposing that  $\dot{\varphi}_i = 0$ .

This is equivalent to studying the fixed points of the system (2.46) and their stability, in terms of  $(r_1, r_2, \theta, \omega_g)$ . In order to do this, we apply a numerical algorithm to calculate the fixed points of the system, in terms of these four

variables. The gradient of the target function for the numerical algorithm is:

$$\nabla \cdot \bar{\mathbf{g}}(r_1, r_2, \theta, \omega_g) = \frac{1}{(8\omega_g)^4} \cdot \quad (2.50)$$

$$\begin{bmatrix} -3r_1^2|\varepsilon_1| + 4\varepsilon_1 & 4\mu_{12}\omega_g c_\theta + 4\mu_{11}s_\theta & -4\mu_{12}r_2\omega_g s_\theta + 4\mu_{11}r_2c_\theta & \frac{r_1^3|\varepsilon_1| - 4\mu_{11}r_2s_\theta - 4\varepsilon_1r_1}{\omega_g} \\ 4\mu_{21}\omega_g c_\theta - 4\mu_{22}s_\theta & -3r_2^2|\varepsilon_2| + 4\varepsilon_2 & -4\mu_{21}r_1\omega_g s_\theta - 4\mu_{22}r_1c_\theta & \frac{r_2^3|\varepsilon_2| + 4\mu_{22}r_1s_\theta - 4\varepsilon_2r_2}{\omega_g} \\ \frac{4(\mu_{12}r_2\omega_g s_\theta - \mu_{11}r_2c_\theta)}{r_1^2} & -\frac{4(\mu_{12}\omega_g s_\theta - \mu_{11}c_\theta)}{r_1} & -\frac{4(\mu_{12}r_2\omega_g c_\theta + \mu_{11}r_2s_\theta)}{r_1} & -\frac{4(\mu_{11}r_2c_\theta - r_1\omega_g^2 - r_1)}{r_1\omega_g} \\ \frac{4(\mu_{21}\omega_g s_\theta + \mu_{22}c_\theta)}{r_2} & -\frac{4(\mu_{21}r_1\omega_g s_\theta + \mu_{22}r_1c_\theta)}{r_2^2} & \frac{4(\mu_{21}r_1\omega_g c_\theta - \mu_{22}r_1s_\theta)}{r_2} & -\frac{4(\mu_{22}r_1c_\theta - r_2\omega_g^2 - r_2\omega_g^2)}{r_2\omega_g} \end{bmatrix},$$

where in the expression the term  $1/8\omega_g$  is multiplied to each row.

The algorithm usually converges to machine precision in less than 10 iterations. The system presents from one to two solutions<sup>5</sup>. We then evaluate the stability of the fixed point in terms of  $r_1, r_2, \varphi_1, \varphi_2$ , calculating the eigenvalues of the Hessian of the system (2.46). The Hessian is:

$$\mathbf{H}(r_1, r_2, \theta, \omega_g) = (8\omega_g)^4 \cdot \quad (2.51)$$

$$\begin{bmatrix} -\frac{3r_1^2|\varepsilon_1| - 4\varepsilon_1}{8\omega_g} & \frac{\mu_{12}\omega_g c_\theta + \mu_{11}s_\theta}{2\omega_g} & -\frac{(\mu_{12}\omega_g s_\theta - \mu_{11}c_\theta)r_2}{2\omega_g} & \frac{(\mu_{12}\omega_g s_\theta - \mu_{11}c_\theta)r_2}{2\omega_g} \\ \frac{\mu_{21}\omega_g c_\theta - \mu_{22}s_\theta}{2\omega_g} & -\frac{3r_2^2|\varepsilon_2| - 4\varepsilon_2}{8\omega_g} & -\frac{(\mu_{21}\omega_g s_\theta + \mu_{22}c_\theta)r_1}{2\omega_g} & \frac{(\mu_{21}\omega_g s_\theta + \mu_{22}c_\theta)r_1}{2\omega_g} \\ \frac{(\mu_{12}\omega_g s_\theta - \mu_{11}c_\theta)r_2}{2r_1^2\omega_g} & -\frac{\mu_{12}\omega_g s_\theta - \mu_{11}c_\theta}{2r_1\omega_g} & -\frac{(\mu_{12}\omega_g c_\theta + \mu_{11}s_\theta)r_2}{2r_1\omega_g} & \frac{(\mu_{12}\omega_g c_\theta + \mu_{11}s_\theta)r_2}{2r_1\omega_g} \\ 8\frac{\mu_{21}\omega_g s_\theta + \mu_{22}c_\theta}{2r_2\omega_g}, & -\frac{(\mu_{21}\omega_g s_\theta + \mu_{22}c_\theta)r_1}{2r_2^2\omega_g}, & \frac{(\mu_{21}\omega_g c_\theta - \mu_{22}s_\theta)r_1}{2r_2\omega_g}, & -\frac{(\mu_{21}\omega_g c_\theta - \mu_{22}s_\theta)r_1}{2r_2\omega_g} \end{bmatrix},$$

where the factor  $8\omega_g$  is distributed in each row. We will discuss extensively the solution in section 2.5.

#### 2.4.1.2 Study of regularity of the perturbation problem

We now discuss under which conditions the system (2.45) is a regular perturbation problem with a stable solution. If such conditions exist and are satisfied, we should be able to:

- determine a solution of the unperturbed problem setting  $\varepsilon = 0$  in (2.45).
- calculate the limit-cycle amplitudes from the standard perturbation problem, that then becomes

$$\dot{\bar{\zeta}} = \varepsilon \bar{\mathbf{g}}_\varepsilon(\bar{\zeta}, t) \quad (2.52)$$

<sup>5</sup>This is a numerical result without proof

We first observe that if such solution exists, the standard perturbation problem (2.52) is simple, and presents the solution ( $r_1 = 2, r_2 = 2$ ). We use this result and check if it is compatible with the unperturbed problem, i.e. if there exist  $\omega_g, \theta$  that satisfy such problem. We begin studying the fixed points of the unperturbed problem, setting  $\varepsilon = 0$  in (2.45), and analyzing the first two equations (2.46.a, 2.46.b):

$$\begin{cases} 0 &= (s_\theta \mu_{11} + c_\theta \mu_{12} \omega \omega_g) \frac{r_2}{2} \\ 0 &= (c_\theta \mu_{21} \omega_g - s_\theta \mu_{22}) \frac{r_1}{2} \end{cases} \quad (2.53)$$

They lead to the solution

$$\tan \theta^\alpha = \frac{\mu_{21}}{\mu_{22}} \quad (2.54)$$

$$\omega_g^\alpha = -\frac{1}{\omega} \frac{\mu_{21}}{\mu_{12}} \frac{\mu_{11}}{\mu_{22}} \quad (2.55)$$

We then consider equations (2.46.c, 2.46.d):

$$\begin{cases} \omega_g^2 - 1 + c_\theta \mu_{11} - s_\theta \mu_{12} \omega \omega_g = 0 \\ \omega_g^2 - \omega^2 + c_\theta \mu_{22} + \mu_{21} \omega_g s_\theta = 0 \end{cases} \quad (2.56)$$

Since there is no simple analytical solution to these equations, we will refer to it as  $(\theta^\beta, \omega_g^\beta)$ . In general, the two solutions of the system (2.56) and (2.53) don't coincide, and only for particular combinations of the parameters  $\mu_{ij}$  we have that

$$\theta^\beta(\mu_{ij}) = \theta^\alpha(\mu_{ij}) \quad (2.57)$$

$$\omega_g^\beta(\mu_{ij}) = \omega_g^\alpha(\mu_{ij}) \quad (2.58)$$

and the perturbed problem converges to the unperturbed problem for  $\varepsilon \rightarrow 0$ .

## 2.4.2 Distinct oscillators

We hypothesize now that the two VdP oscillate at their natural frequencies, respectively 1 and  $\omega$ , and discuss the stability of this solution. We proceed in a similar way to the previous section, substituting in the system (2.30) the following

trial solution:

$$\begin{cases} x_1 = r_1 \sin(t - \varphi_1) \equiv r_1 s_1 \\ y_1 = r_1 \cos(t - \varphi_1) \equiv r_1 c_1 \\ x_2 = r_2 \sin(\omega t - \varphi_2) \equiv r_2 s_2 \\ y_2 = \omega r_2 \cos(\omega t - \varphi_2) \equiv \omega r_2 c_2 \end{cases} . \quad (2.59)$$

We obtain the system of equations:

$$\begin{cases} \dot{r}_1 = \mu_{11} r_2 c_1 s_2 + \mu_{12} \omega r_2 c_2 c_1 + \varepsilon_1 f_2^1 c_1 \\ \omega \dot{r}_2 = \mu_{22} r_1 c_2 s_1 + \mu_{21} r_1 c_2 c_1 + \varepsilon_1 f_4^1 c_2 \\ \dot{\varphi}_1 = \mu_{11} \frac{r_2}{r_1} s_2 s_1 + \mu_{12} \omega \frac{r_2}{r_1} c_2 s_1 + \frac{\varepsilon_1}{r_1} f_2^1 s_1 \\ \omega \dot{\varphi}_2 = \mu_{22} \frac{r_1}{r_2} s_2 s_1 + \mu_{21} \frac{r_1}{r_2} c_1 s_2 + \frac{\varepsilon_1}{r_2} f_2^1 s_2 \end{cases} \quad (2.60)$$

We observe that if  $\mu_{ij} = O(\varepsilon)$ , this is a perturbation problem in standard form, as defined in (1.20). We now proceed applying the averaging method separately on the two oscillators. In particular, we choose as averaging periods the natural periods of the two oscillators.

The average of the nonlinear terms is the same of the previous section, as in (2.44), and also equations (2.39) hold. The only difference regards the mixed terms like  $s_1 c_2$ , that present zero average. This leads to two non-interacting oscillators,

$$\begin{cases} \dot{r}_1 \omega_g = \varepsilon_1 \frac{r_1}{2} - |\varepsilon_1| \left(\frac{r_1}{2}\right)^3 \\ \dot{r}_2 \omega_g = \varepsilon_2 \frac{r_2}{2} - |\varepsilon_2| \left(\frac{r_2}{2}\right)^3 \\ \dot{\varphi}_1 \omega_g = 0 \\ \dot{\varphi}_2 \omega_g = 0 \end{cases} \quad (2.61)$$

that tend to the natural amplitudes of  $r_1 = r_2 = 2$ , with constant phases  $\varphi_1, \varphi_2$  undefined, depending on the initial conditions. It hasn't been investigated yet if, for small enough coupling, this is a solution of the problem.

## 2.5 Discussion of the solution

In this section we investigate the solutions of the system (2.46). We first discuss the solution for values of  $\mu_{ij}$  on a line in the 4-dimensional parameters space, for increasing values of their distance  $\bar{\mu}$ <sup>6</sup> from the origin. Then we will consider the particular case of velocity coupling, at a fixed distance from the origin.

The case of displacement coupling is expected to be similar to the case of velocity coupling, with a shift of  $\pi/4$  of the parameter space  $(\mu_{11}, \mu_{22})$  with respect to  $(\mu_{12}, \mu_{21})$  and a rescaling due to  $\omega$  appearing as a factor in the coupling coefficient  $\mu_{12}\omega$ . For this reason it will not be investigated.

We will finish comparing the results of the averaging method with respect to the simulations on a disc of the  $(\mu_{12}, \mu_{21})$  plane.

### 2.5.1 Dependence on the distance from the origin

I consider the same configuration for the simulation results in presented in figures 2.2, 2.3, 2.4, 2.5, with the space of parameters defined in (2.27).

A solution of the system (2.46) can always be found, but it is stable only above a certain value of the coupling intensity  $\bar{\mu}$ . We present in figure 2.6.a the real part of the eigenvalues describing the stability of the system. I have reported with a vertical line the critical value of  $\bar{\mu} \approx 0.0877$  above which the system doesn't present unstable solution, i.e. when all eigenvalues are not positive. The existence of an eigenvalue with null real part is not important at this stage, and will be discussed later on. The simulations match reasonably this value: from figure 2.3 it can be seen that the critical value of  $\bar{\mu}$  for a stable solution is between 0.0360 and 0.0620. Although more investigations are required to confirm it more accurately, the instability of the slow flow seems to be correlated to the existence of a quasi-periodic solution, and vice-versa.

Above such critical value, the solution is stable, and the predicted limit cycles amplitudes  $r_1, r_2$  are reported as horizontal lines in the time series, as in figure 2.2. For a certain range of  $\bar{\mu}$ , the precision of the predicted limit-cycle amplitudes is within 15% of the measured amplitudes of the two VdP, in excess. This is due to the fact that the trial solution (2.31) doesn't consider higher harmonics, that, as commented in section 2.3 about figures 2.4 and 2.5, become stronger with  $\bar{\mu}$ .

---

<sup>6</sup>defined in equation (2.28) with a standard Euclidean norm

These results are all condensed in figure 2.6.b, where we report the precision of the averaging method as a function of  $\bar{\mu}$ . The precision of the predicted global frequency seems to not be influenced much by the nonlinearity of the system, and is very close to the measured entrained frequency, with an error of around 3%.

In figure 2.7 I report the precision of 15 simulations for 15 randomly generated values of  $\mu_{ij}$  such that  $0.2 < \mu_{ij} < 0.4$  for each parameter. The precision is within the 3% of the measured final state.

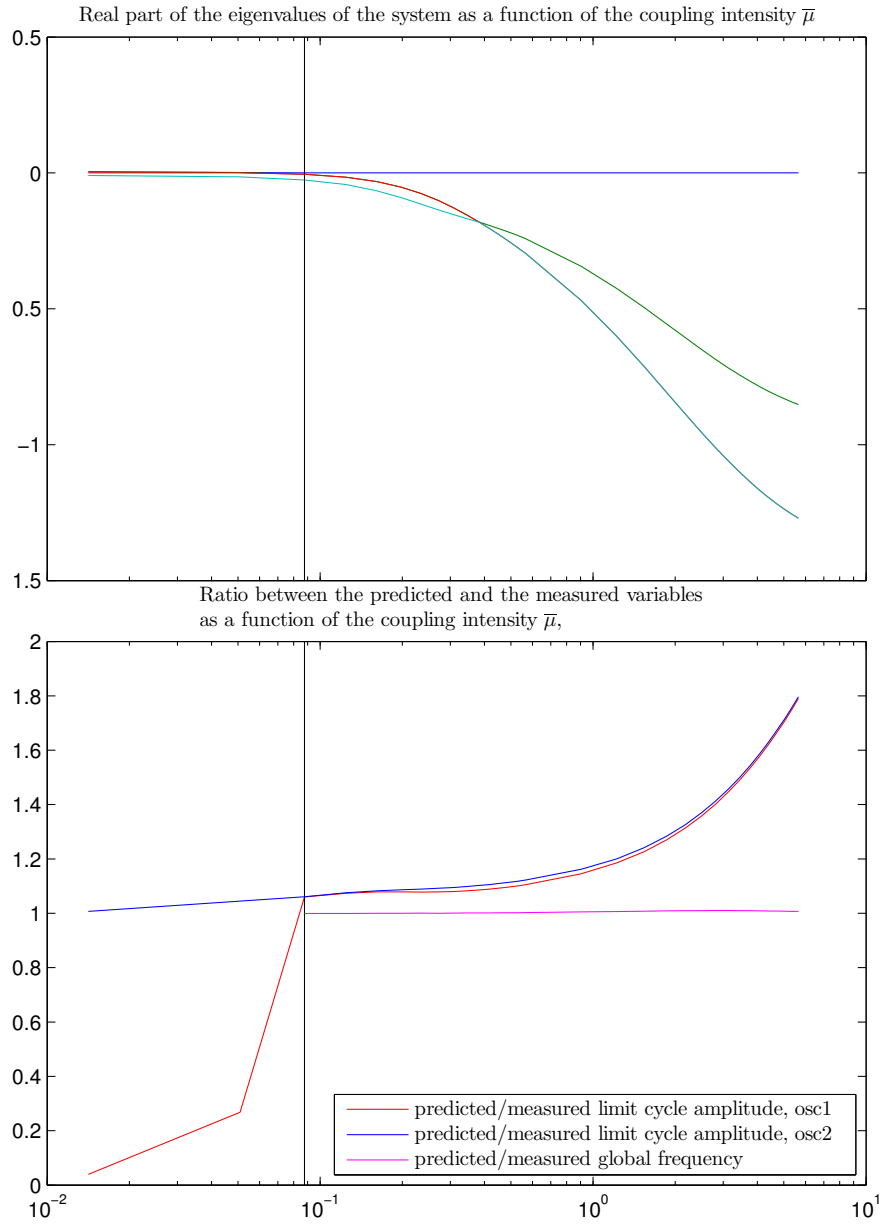


Figure 2.6: Precision of the averaging method. For values of  $\bar{\mu}$  to the left of the vertical black line, the solution is unstable and the simulations don't present an entrained solution. For large values of the coupling  $\bar{\mu}$ , the precision drops due to higher order harmonics.

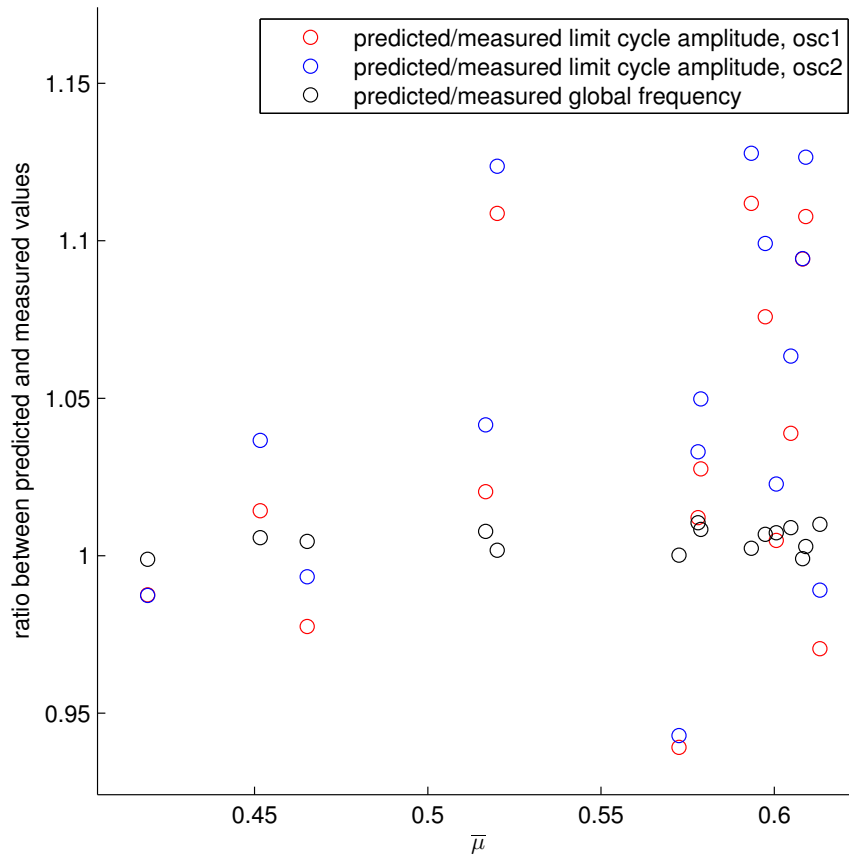


Figure 2.7: Precision of the averaging method for 15 randomly generated coupling cases, such that  $0.2 < \mu_{ij} < 0.4$ . The precision of the method is much higher in this interval.

## 2.5.2 The case of velocity coupling

We now study the system where the averaging method seems to be reliable, fixing  $\bar{\mu} = 0.3$ , and considering the following parameter space:

$$\mu_{12} = 0.3 \sin \alpha_i \quad \mu_{21} = 0.3 \cos \alpha_i \quad \mu_{11} = 0 \quad \mu_{22} = 0, \quad (2.62)$$

$$\alpha = \frac{\pi}{180}i, \quad i = 0, 1, \dots, 180. \quad (2.63)$$

We restrict the study to the first two quadrants exploiting a symmetry of the system (see the discussion below equation (2.46)). The system presents one or two solutions. In figure 2.8 we report, as functions of  $\alpha$ , the real parts of the four eigenvalues of the two solutions. The left picture refers to the most stable solution  $sol_1$ , while the right picture to the least stable  $sol_2$ . This second solution exists only in a subdomain, that is approximately  $\mathcal{D} \approx [1.8, 3]$  radians. Both solutions always present an eigenvalue  $\lambda_1$  with null real part. The respective eigenvector  $v_1$  presents components  $(0, 0, \nu, \nu)$ , and expresses a synchronous shift of the phases of both oscillators of the same quantity, without affecting the global frequency  $\omega_g$  and the two limit-cycle amplitudes  $r_1, r_2$ . Moreover,  $sol_1$  is neutrally stable in the whole domain, while  $sol_2$  is neutrally stable only in  $\mathcal{D} \ni \mathcal{D}' \approx [2.1, 2.8]$ , being unstable in  $\mathcal{D} \setminus \mathcal{D}'$ . Since this neutrally stable eigenmode regards only the possibility of the system to undergo synchronization, we will now discuss the stability considering only the other three eigenvalues.<sup>7</sup>

We now consider only stable solutions, i.e.  $sol_1$  in the whole domain, and  $sol_2$  in  $\mathcal{D}'$ . We plot in figure 2.9 the four variables describing the final state of the system, employing dashed lines for the less stable solution  $sol_2$ .

---

<sup>7</sup>This is practically carried on discarding eigenvalues with real part smaller than 100 times the machine precision.

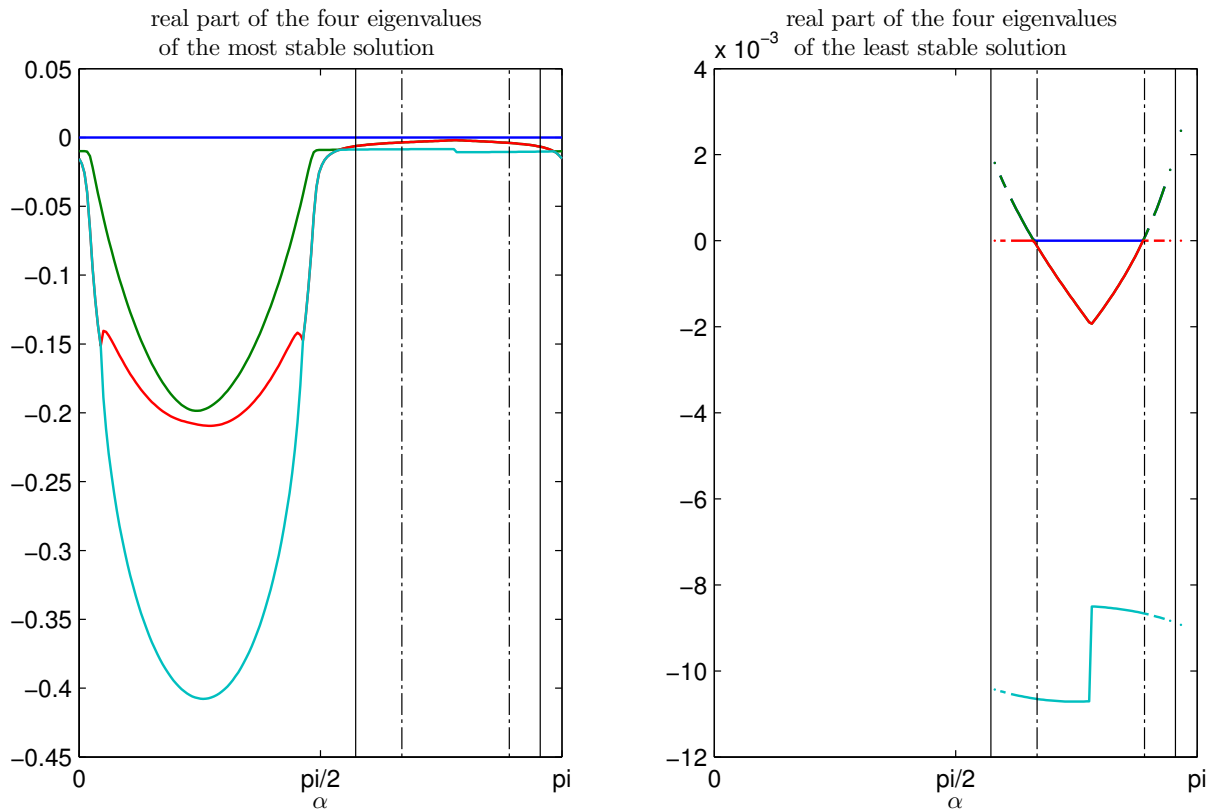


Figure 2.8: In the figure are reported the real parts of the four eigenvalues of the most stable solution  $sol_1$  (left) and the least stable solution  $sol_2$  (right). The vertical continuous and dashed lines describe the two domains  $\mathcal{D}$  and  $\mathcal{D}'$ , respectively of existence and of stability of the  $sol_2$ . Note that the two vertical axis present a different scale.

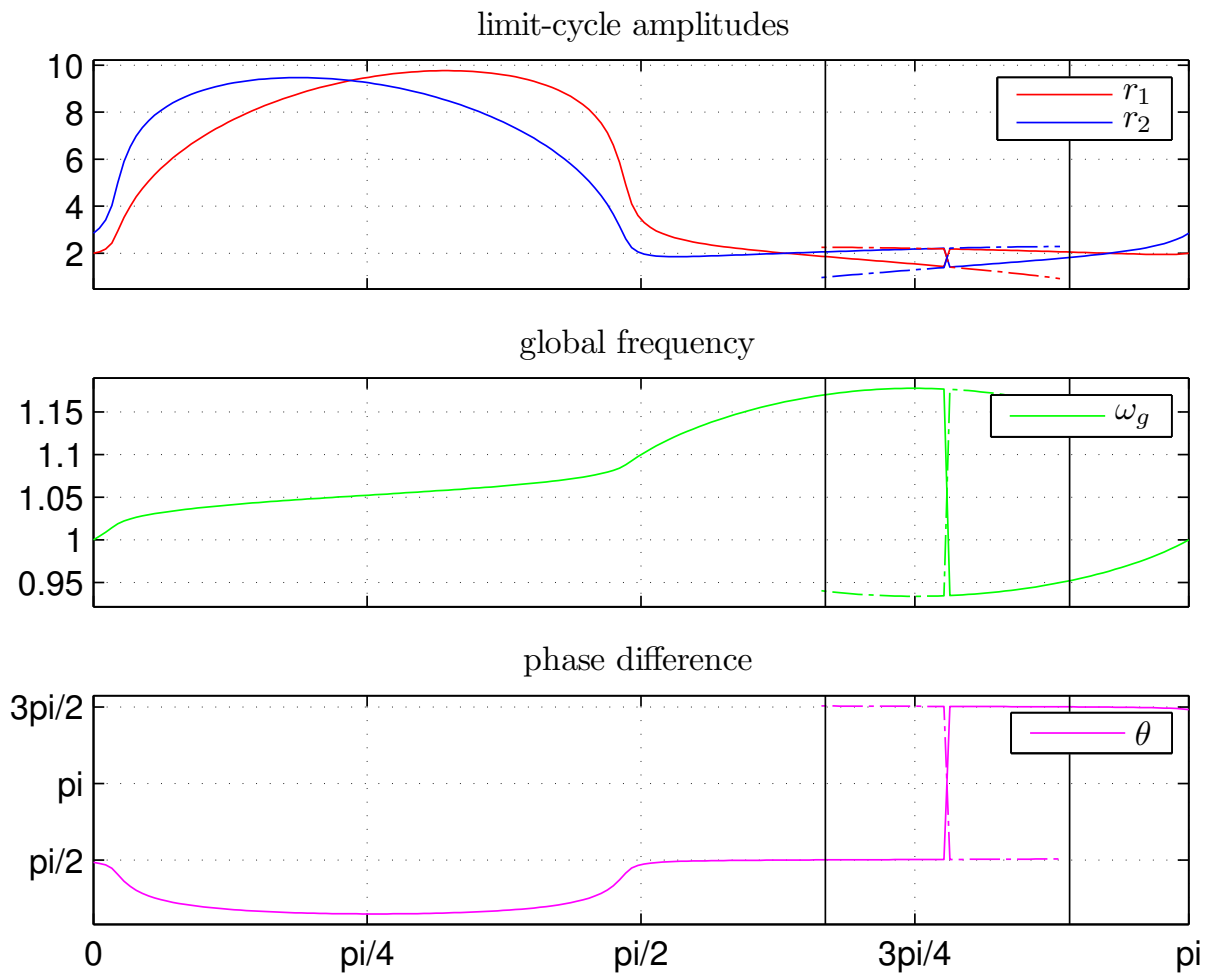


Figure 2.9: Stable solutions of the slow flow. The least stable solution is reported with a dashed line in the domain  $\mathcal{D}'$  delimited by the two black vertical lines. Observe the sharp jump in all the four final-state variables, around  $\alpha \approx 2.4485$  radians

### 2.5.3 Limit-cycle amplitudes for the velocity coupling case

Finally we present a comparison between the results of the simulations and the predicted solutions from the averaging method, on a disc of the  $(\mu_{12}, \mu_{21})$  space, considering the subset of parameters described by:

$$\begin{cases} \mu_{12} = d \sin \alpha \\ \mu_{21} = d \cos \alpha \\ \mu_{11} = 0 \\ \mu_{22} = 0 \end{cases} \quad \begin{cases} \alpha \in [0 \ \pi] \\ d \in [0 \ 1/2] \end{cases} \quad (2.64)$$

To approach numerically the problem, we run the simulations for  $\alpha$  and  $d$  linearly spaced in their intervals of definition, for 12 values of  $\alpha$  and 16 values of  $d$ . We then calculate the predicted solution with the averaging method on that grid. A qualitative comparison between the simulation results and the most stable solution  $sol_1$  and the least stable solution  $sol_2$  of the averaging method are reported in figure 2.10 and 2.11 respectively. There is good agreement in figure 2.10, with the exception of a zone in the second quadrant, where the simulation behaves like  $sol_2$ . This zone corresponds to the domain  $\mathcal{D}'$ , delimited by the two black vertical lines in figure 2.9.

To discuss the precision of predicted solutions we consider the ratio between the values from the left and from the right plot of the two figures. In figures 2.12 and 2.13 we report the two ratios  $q_1$  and  $q_2$  between the measured final state and the predicted final-states  $sol_1$  and  $sol_2$ . To investigate if the simulations don't behave at all like any of  $sol_1$  and  $sol_2$ , we report in figure 2.14 the ratio between the two  $q_1, q_2$  that is closer to unity, to understand of how far from the closest predicted value is the simulation. The predicted values are quite close to the measured ones, and the error becomes larger in the first quadrant, where the final amplitudes are bigger and the nonlinear effects are stronger. This seems to affect specifically the precision of the global frequency, that decreases getting further from the origin.

Recalling the precision of 16 simulations ran with random parameters in  $0.1 < \mu_{ij} < 0.3$  in figure 2.7, it seems reasonable to expect that the averaging method is a good approximation of the final state of the system in the spherical shell of radii  $\bar{\mu}$  equal to 0.1 and 0.3. Starting from this approximate result, it is

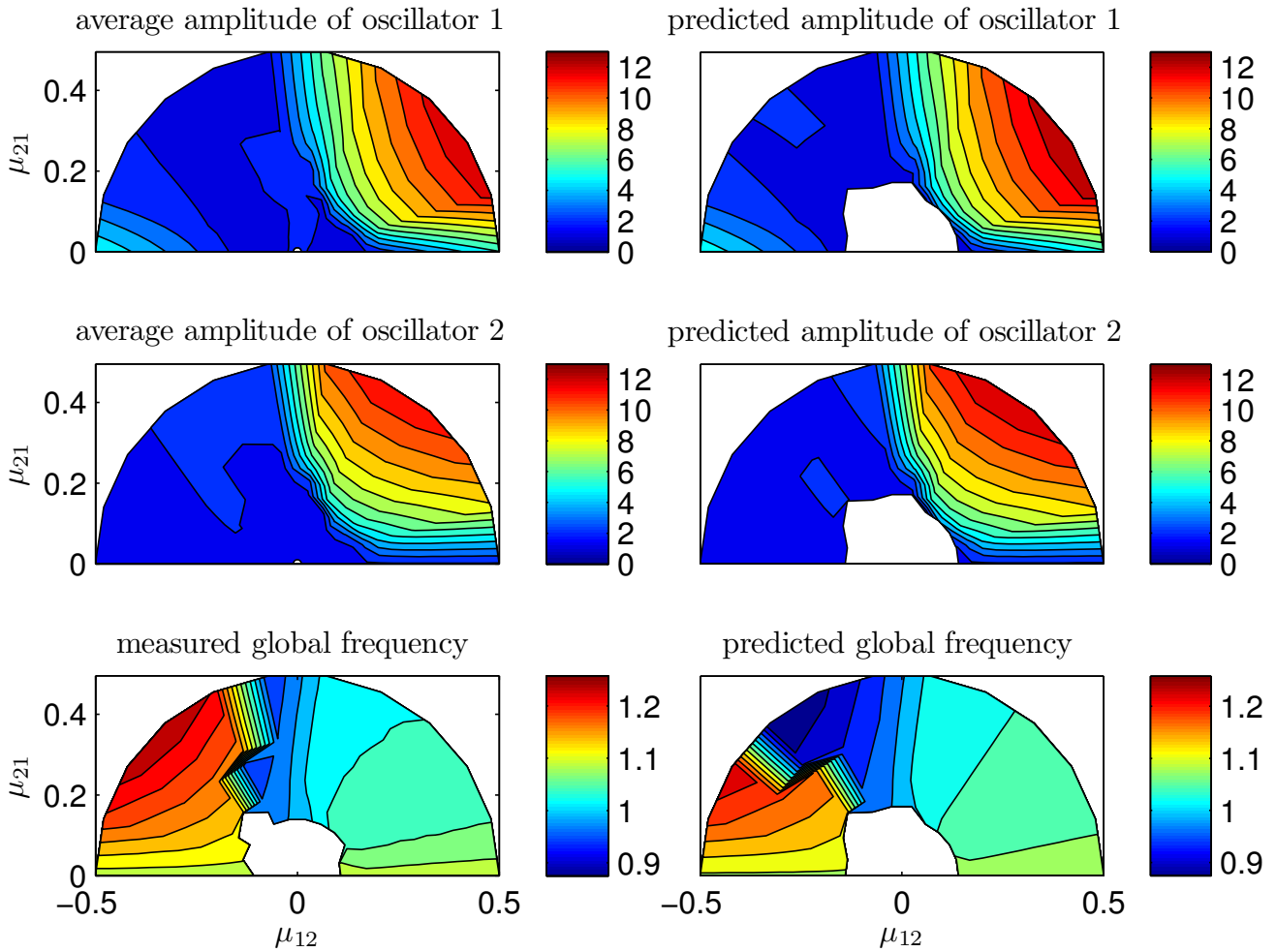


Figure 2.10: Comparison of the simulations (left) with the most stable solution  $sol_1$  of the averaging method (right). Observe the anomaly in the second quadrant of the bottom plot.

possible to apply a continuation tool to the system that takes into account higher harmonics. These tools are computationally more expensive, and either apply a shooting technique or the harmonic balance method. To check the results here presented, we have successfully applied a variant of the latter[2], and were able to confirm the existence of the two distinct stable limit-cycles of the system discovered with the averaging method, and how these two limit-cycles become unstable as  $\bar{\mu}$  approaches zero.

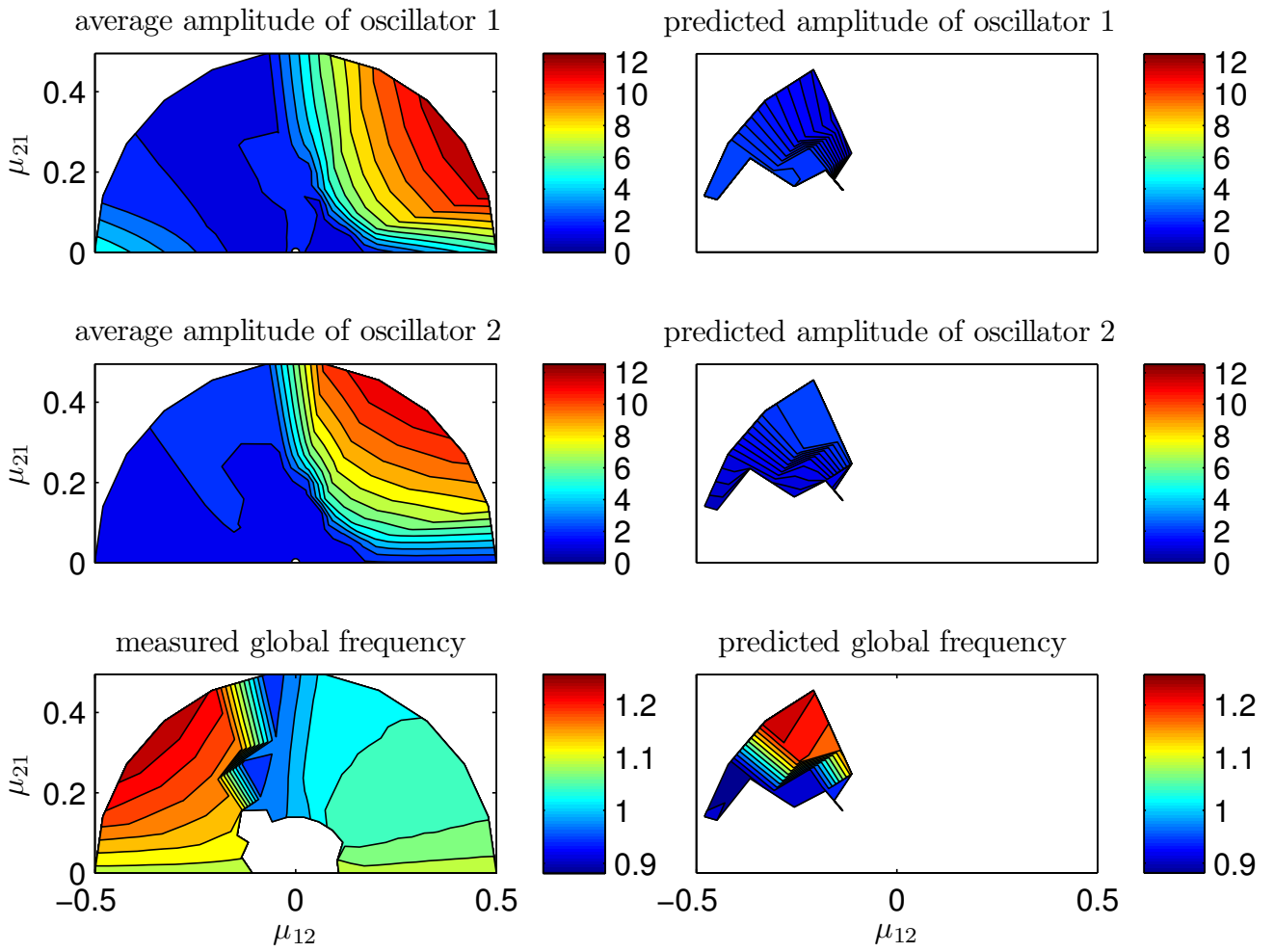


Figure 2.11: Comparison of the simulations (left) with the least stable solution  $sol_2$  of the averaging method (right), that doesn't exist in the whole domain.

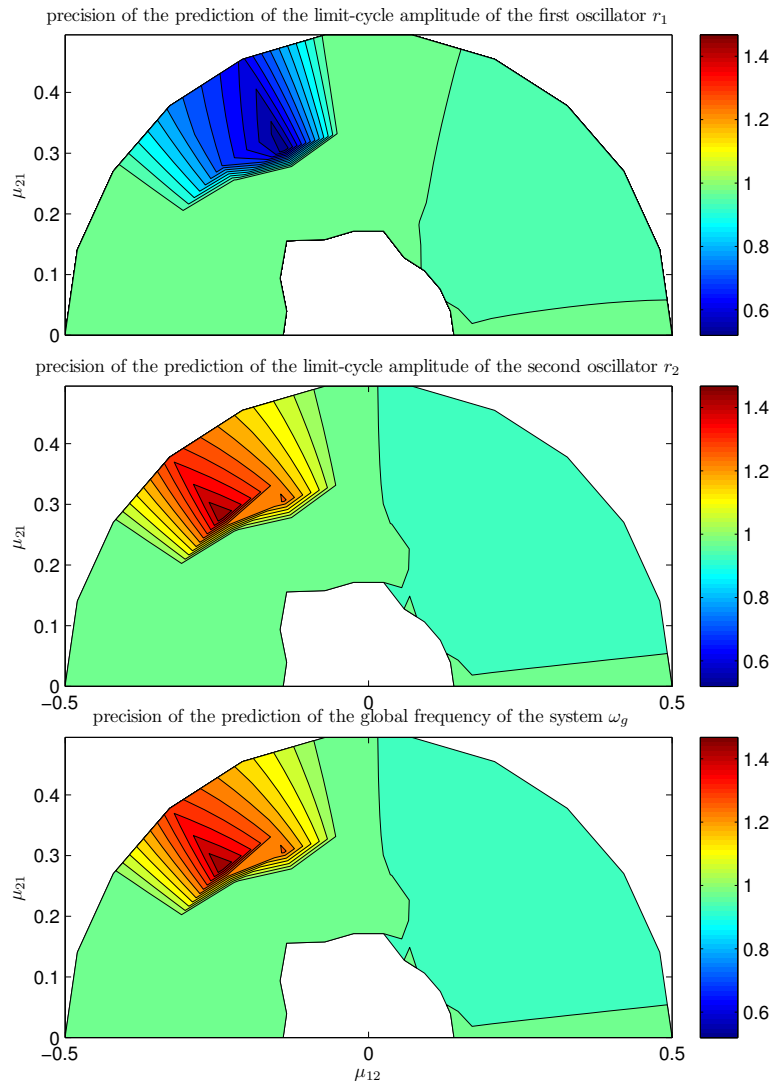


Figure 2.12: ratio between the measured value from the simulation and the solution  $sol_1$  applying the averaging method.

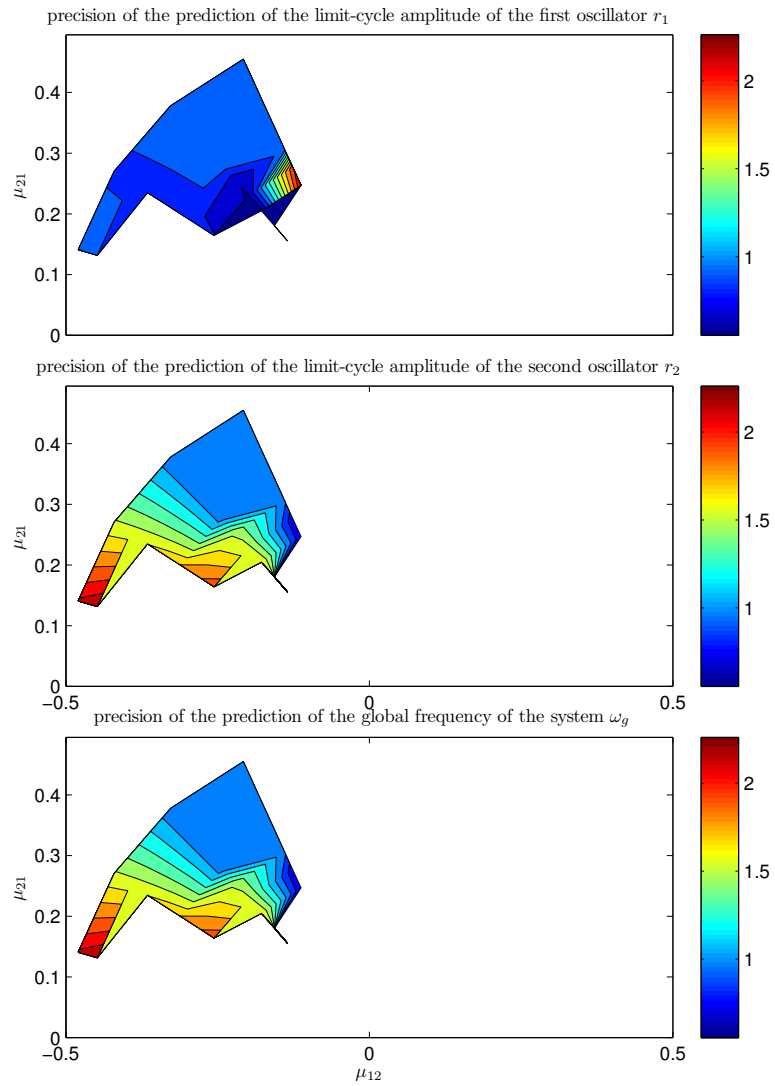


Figure 2.13: ratio between the measured value from the simulation and the solution  $sol_2$  applying the averaging method.

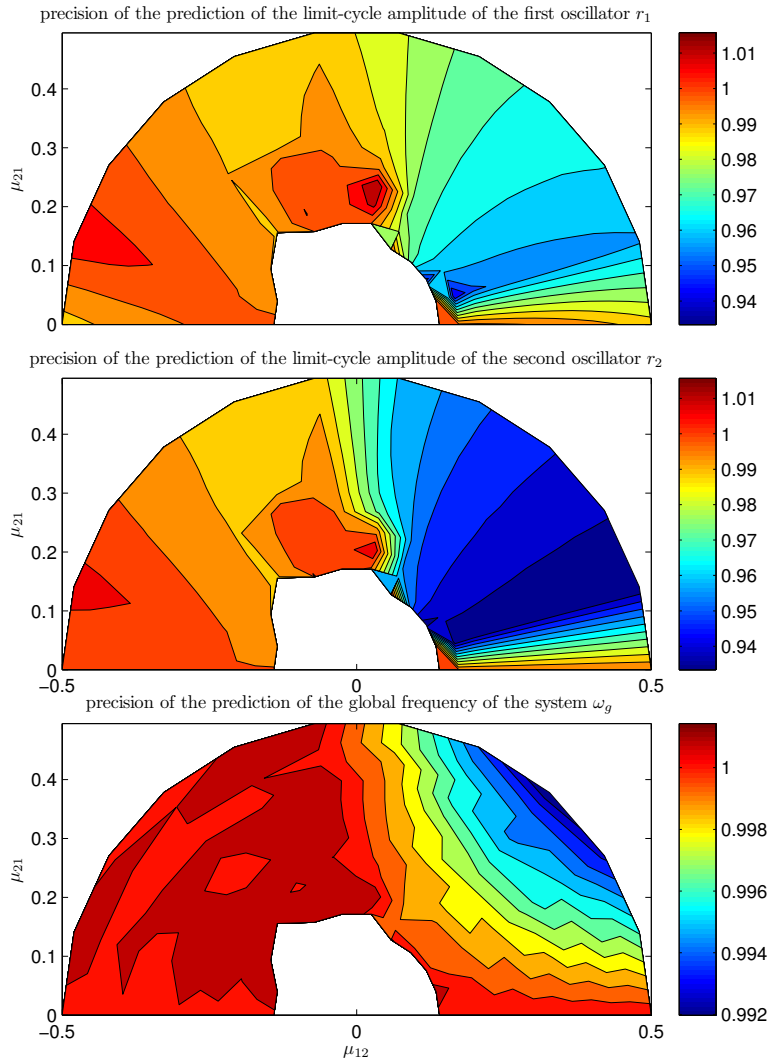


Figure 2.14: ratio between the measured value and the closest solution among  $sol_1$  and  $sol_2$ .

# Bibliography

- [1] Alexander Balanov, Natalia Janson, Dmitry Postnov, and Olga Sosnovtseva. *Synchronization: From simple to complex*. 2009.
- [2] Bruno Cochelin and Christophe Vergez. A high-order purely frequency-based harmonic balance formulation for continuation of periodic solutions. *arXiv*, 2009.
- [3] D W Jordan and P Smith. *Nonlinear differential equations, and introduction for scientists and engineers*. 2007.
- [4] Larry Li and M.P. Juniper. Lock-in and quasiperiodicity in hydrodynamically self-excited flames : experiments and modelling. *Proceedings of the combustion institute*, 34, 2012.
- [5] Arkady Pikovsky, Michael Rosenblum, and Jurgen Kurths. *Synchronization, a Universal Concept in Nonlinear Sciences*. 2001.
- [6] Ubaid Ali Qadri, Mistry Dhiren, and M.P. Juniper. Structural sensitivity of spiral vortex breakdown. Under review for publication. *Journal of Fluid Mechanics*, 2012.
- [7] Balthasar Van Der Pol. A theory of the amplitude of free and forced triode vibrations. *Radio Review*, 1:701–710,754–762, 1920.

